Deep Well Injection of Liquid Radioactive Waste at Krasnoyarsk-26:

Analysis of Hypothetical Scenarios
Volume II

Keith L. Compton
Vladimir Novikov
Frank L. Parker

RR-01-01
February 2001

International Institute for Applied Systems Analysis, Laxenburg, Austria
Tel: +43 2236 807 Fax: +43 2236 73148 E-mail: publications@iiasa.ac.at
Web: www.iiasa.ac.at

International Standard Book Number 3-7045-0140-9

Cover design by Anka James. The cover represents a cross-section through the geological strata that compose the disposal site at Krasnoyarsk-26.

Printed by **Rema***print*, Vienna.

Contents

Acknowledgments

This work could not have been accomplished without the help and cooperation of the Ministry of Atomic Energy of the Russian Federation (Minatom) and the Russian Academy of Sciences and their institutes. Participating institutions include the Mining and Chemical Combine (MCC), the All-Russian Design and Research Institute of Production Engineering (VNIPIPT), the regional administration of the Krasnoyarsk Krai, and the Institute of Geology of Ore Deposits, Petrography, Mineralogy and Geochemistry (IGEM). Among those participating were Nicolai Egorov, deputy minister of Minatom; Vassili Zhidkov and Boris Segaev of the MCC; Andrei Rybalchenko of VNIPIPT; Nicolai Abramov of the regional administration of the Krasnoyarsk Krai; Vasiliy Velichkin, Aleksandr Pek, and Victor Malkovsky of IGEM; and Yuri Gorlinskii of the Russian Research Center "Kurchatov Institute."

We would also like to acknowledge the work of the organizations of the Russian Federation and the former Soviet Union that have contributed to the current store of knowledge about the site. Although it is not possible to list all such organizations, special acknowledgement is due to the Gidrospetsgeology of the Ministry of Geology for the collection of geological data and to the Institute of Physical Chemistry of the Russian Academy of Sciences, which has studied the chemistry of the wastes and the waste–rock interactions.

The work was undertaken jointly by the members of the Radiation Safety of the Biosphere (RAD) Project at the International Institute for Applied Systems Analysis (IIASA) and by Russian specialists from IGEM, VNIPIPT, and the MCC. Although the main report is being issued by IIASA, the work has been a joint effort. The studies of IIASA, IGEM, and VNIPIPT were performed in parallel. Journal articles summarizing major results of the parallel studies were published in Parker *et al.* (1999) and Parker *et al.* (2000). The current volume is an IIASA Research Report reflecting primarily RAD Project activities in this study. However, it reviews and incorporates selected results obtained by IGEM and VNIPIPT. The reports of these individual research groups are available from the IIASA Library.

We would like to thank the US Department of Energy for funding this study under Grant No. DE-FG02-96EW13112, Amendment No. A001 and A003, and Mr David Huizenga, acting deputy assistant secretary of the Office of Nuclear Material and Facility Stabilization, for sponsorship of the work. We would also like to thank Gordon J. MacDonald, former director of IIASA, for his interest in the work; Academician Nicolai Laverov, vice president of the Russian Academy of Sciences, and the late Nicolai Egorov, deputy minister of Minatom, for their help in easing the availability of data; and Academician Eugene Velikhov, president of the Russian Research Center "Kurchatov Institute," for his interest in the study.

We would also like to thank Ms Ulrike Neudeck of the IIASA RAD Project for her administrative support of this project, as well as the other members of the IIASA support staff for their assistance in the completion of this study.

1
Introduction

The Mining and Chemical Combine (MCC), located approximately 60 km north of the city of Krasnoyarsk, is one of two major sites in the Russian Federation where liquid radioactive wastes (LRW) are disposed of by deep well injection. Disposal of LRW at the MCC through the use of deep well injection started in 1967. The Severny ("Northern") site, approximately 15 km north of the MCC, was launched after the completion of special geological surveys and explorations performed by institutions of the Ministry of Geology and Russian Academy of Sciences. The site was designed by Minatom institutions. As of 1995, 5 million cubic meters (m^3) of LRW had been injected into two deep aquifers at the site. The waste includes both radioactive fission products and nonradioactive chemicals used in reprocessing of spent fuel. The total activity, decay corrected to 1995, is approximately 250 million Curies (Ci). Detailed information about radioactive waste disposal at the Severny site is presented in Volume I of this report (Compton *et al.*, 2000), which includes an evaluation of the safety of the site under normal post-operational conditions. For further information on the background data contained in Chapter 2 of that report, see Appendix I. The subject of the current report is the likelihood and consequences of hypothetical accidents and extreme natural events after site decommissioning, including a brief overview of the factors involved in the development of decommissioning plans at the site.

2
Discussion of Hypothetical Accidents and Problems

The primary discussion of hypothetical accidents and problems scenarios was prepared by the All-Russian Design and Research Institute of Production Engineering (VNIPIPT). In their Phase I report (VNIPIPT, 1998), potential problems were divided into two categories: operational and post-operational. Operational problems include

- damage to surface equipment and wells,
- development of potentially dangerous conditions in a reservoir horizon due to disposal operations,
- mistakes during the siting, design, and operation of the repository, and
- natural disasters and natural accidents during operation.

Post-operational problems include

- abnormal migration of wastes with the flow of underground waters or vertical redistribution of wastes,
- degradation of the condition of decommissioned wells,
- intrusion into the waste horizons by future generations, and
- natural changes of the geologic environment.

This work focuses on the second class of problem scenarios, that is, hypothetical conditions that could arise after decommissioning of the site. The post-operational problems listed above were reviewed and two worst-case scenarios were selected for analysis. The first scenario selected was that of an inadvertent intrusion into the waste disposal aquifers by future generations and the use of the contaminated groundwater as a sole source of drinking water. The second scenario selected was the failure of the confining ability of the fault zone bounding the site as a result of future tectonic activity and the consequent migration of wastes toward

the Yenisei River. In addition, a sensitivity analysis was carried out to examine the significance of uncertainty in hydrological parameters in Horizon I.

The scenario in which the confining ability of the clay layer overlying Horizon I is degraded (e.g., by an unsealed well drilled into Horizon I or the degradation of well sealing in a Horizon I well) was not fully evaluated in this study. VNIPIPT performed an evaluation (VNIPIPT, 1998) based on the results of studies at Moscow University and the Institute of Physical Chemistry which concluded that degradation of the conserved wells will not occur after site decommissioning. The VNIPIPT study also evaluated the flow that could occur under injection conditions and concluded that approximately 8 m^3 could flow to an overlying horizon over approximately 30 years (approximately 0.8 liters per day [L/d], under the assumptions of the analysis). However, an evaluation of resulting contamination levels in the upper horizon and the doses that could be received was not conducted.

However, the scenario of an unsealed borehole (resulting either from mistakes during decommissioning or from future drilling leaving an unsealed puncture in the confining layer) was not evaluated. Additional data on the hydrologic parameters of the aquifers overlying the disposal ground (transmissivity, water head, etc.) and on the type of potential interconnections (e.g., fully penetrating all aquifers, such as an unsealed shaft through all horizons, versus a partially penetrating interconnection linking Horizon I with Horizon III through the interior of a well casing) are necessary for a full examination of this problem.

3

Waste Transport in Horizon I: Sensitivity Analyses

The transmissivity and porosity of aquifers are typically among the most important parameters in modeling the migration of contaminated groundwater. Unfortunately, however, these parameters are often characterized by a relatively high level of uncertainty. This is true at the Severny injection site, where no data on spatial variability of porosity and only limited information on the pumping tests used to derive transmissivity values were available. The sensitivity of the migration patterns of the intermediate-level waste (ILW) and high-level waste (HLW) in Horizon I to changes in these parameters was therefore analyzed by the Institute of Geology of Ore Deposits, Peterography, Mineralogy and Geochemistry, or IGEM (1999a) using the code developed in Phase I (IGEM, 1998b) for modeling migration of dense wastes. Their results are summarized here.

The first sensitivity analysis considered the sensitivity of the waste movement to changes in porosity. The nominal value of porosity for the entire aquifer was 0.07 (VNIPIPT, 1998). As a decrease in porosity leads to an increase in groundwater velocity, it was decided to examine the effect of halving the porosity from 0.07 to 0.035. The results for both cases are shown in *Figure 3.1*. A simple application of Darcy's law would imply that the distance traveled by the plume should increase by a factor of two. However, only a marginal increase in the spread of the plume is shown in *Figure 3.1*. The explanation for this seeming anomaly is that density effects dominate regional head-driven flow patterns in the IGEM model of waste transport, causing the dense saline wastes to settle in the syncline region north of the disposal area.

The second analysis examined the sensitivity of model results to changes in transmissivity. Transmissivity values determined from pumping tests at 10 different wells were given in VNIPIPT (1998). The sensitivity analysis was conducted by performing a new calibration of the model (see IGEM, 1998b) with increased values of transmissivity. Each reported value of transmissivity was increased by a factor of two, and the calibration procedure was reapplied to obtain a new distribution for the transmissivity and leakage parameter. The results of modeling the

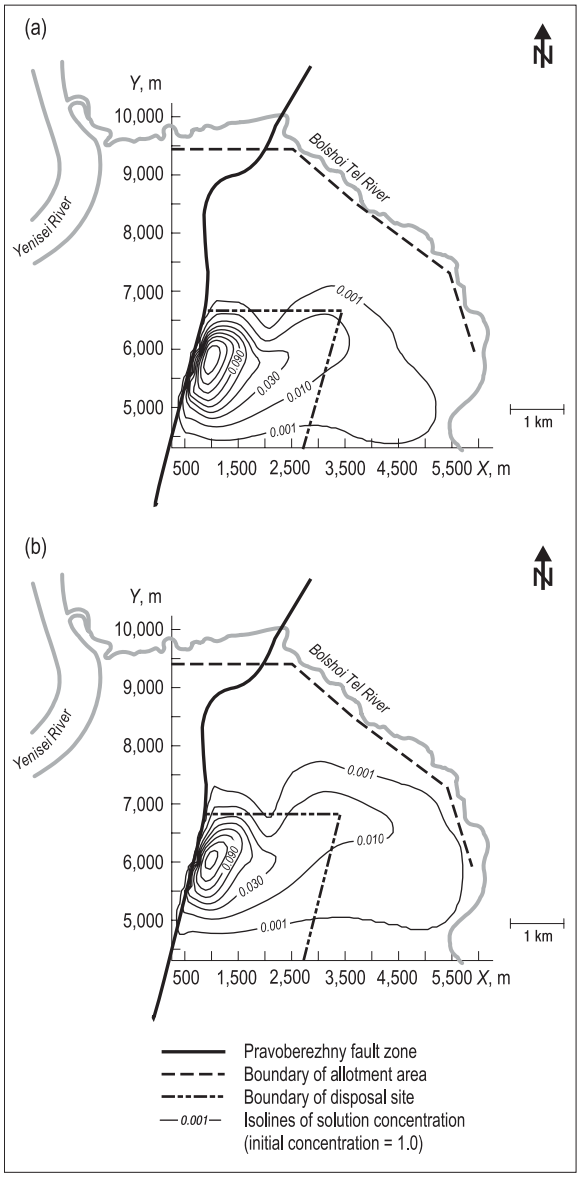

Figure 3.1. Position of waste plume at 1,000 years: (a) porosity $n = 0.07$; (b) porosity $n = 0.035$.

transport of the dense Horizon I wastes using the altered transmissivity distribution are shown in *Figure 3.2*. Again, it can be seen that the movement of the waste plume is slower than might be expected. The explanation is the same: density-driven flow dominates regional groundwater flow for the dense wastes, causing them to settle in the depression north of the site. In addition, the recalibration caused changes

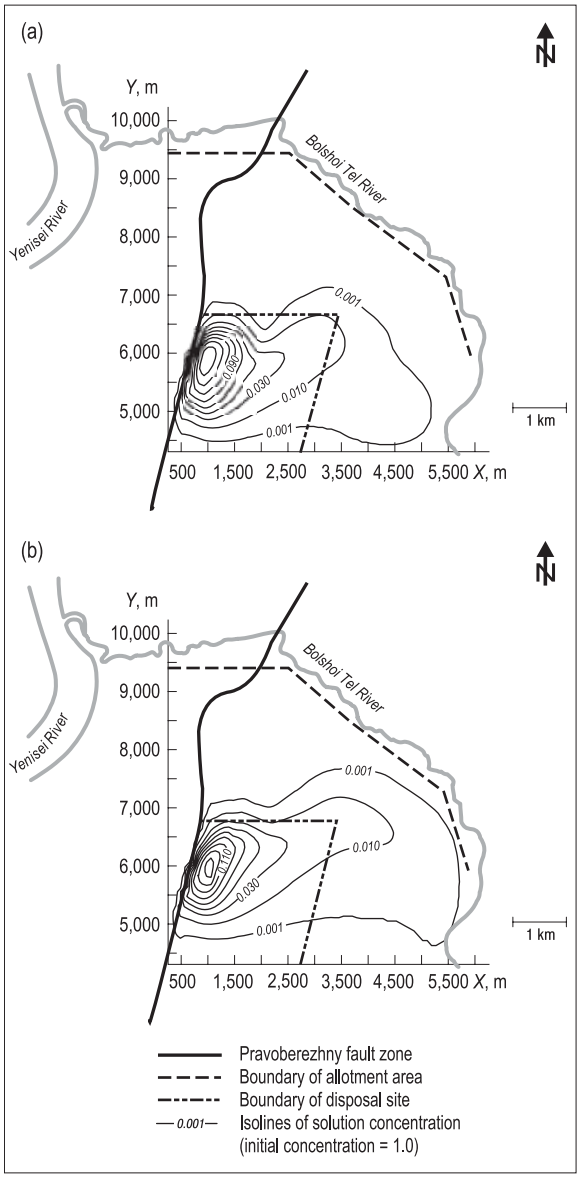

Figure 3.2. Position of waste plume at 1,000 years: (a) nominal transmissivity; (b) 2× nominal transmissivity.

in the leakage time of wastes from Horizon I to Horizon II. The effects of these changes are seen in *Figure 3.3*. It can be seen that the distribution of the leakage time drops rather significantly as a result of model recalibration with increased transmissivities. However, in all areas of the aquifer, leakage through the confining layer requires over 1,000 years.

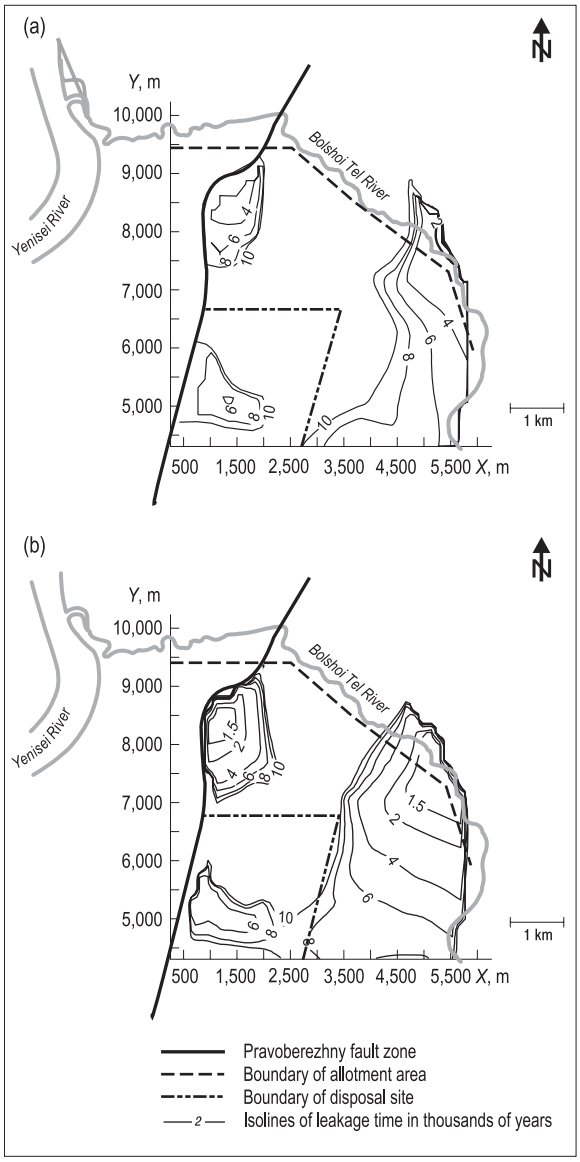

Figure 3.3. Leakage time through confining layer: (a) nominal transmissivity; (b) $2\times$ nominal transmissivity.

4

Inadvertent Intrusion into Disposal Horizons

Analysis of the inadvertent intrusion scenario was conducted in two parts. The first part is a quantitative analysis of the consequences of a failure of institutional controls, leading to the use of drinking water from a well located in a disposal horizon. The second part is a qualitative analysis of the likelihood of such an intrusion. Since the risk posed by the contaminants in the subsurface is a function of the probability of exposure as well as the consequences of exposure, a formal analysis of the likelihood of exposure gives a more complete picture of the risks.

For the Phase II analysis presented in this volume, the numerical model used for the base case (discussed in Volume I of this report, see Compton *et al*., 2000) was updated to include the effects of radioactive decay and sorption in a more comprehensive manner. Another refinement to the original model was the more limited area of potential discharge of Horizon I, based partially on the results of the modeling performed by IGEM in Phase I studies (IGEM, 1998a) and partially on IIASA interpretation of the input data. As a result of these changes, the model now simulates flow passing underneath the Bolshoi Tel River and continuing to flow north toward the Kan River. In addition, the modeled area of Horizon I was expanded to include the upthrown block and the Yenisei River. The third refinement to the base case model was the inclusion of dispersion and molecular diffusion.

The inadvertent intrusion scenario assumes that a well is drilled into the disposal horizons and the water is used for drinking water. The exposure point is thus the contaminated water in the aquifer itself, and the exposure pathway is use of contaminated water as drinking water. Evaluation of doses due to agricultural pathways was not carried out because of a lack of agricultural data for the region. These doses could be significant.

Since the location of future wells cannot be determined, the analysis was performed in two conceptual steps. The first step was to model the transport of contaminants in the subsurface. The transport analysis is thus identical to the transport analysis conducted for the base case. However, unlike in the base case, a dose factor was developed and applied directly to the subsurface contaminant concentrations.

This allows the creation of a plot of potential total drinking water doses at all points in the aquifer at a given time. Dose factors are based on the 50-year committed effective dose equivalent due to ingestion of contaminated groundwater for a period of one year. Development of the subsurface dose plots permits a determination of the areas that may yield unacceptable doses if wells are placed there in the future.

4.1 Consequence Analysis

Modeling was carried out using MODFLOW-96 (McDonald and Harbaugh, 1988; Harbaugh and McDonald, 1996) and MOC3D (Konikow *et al.*, 1996). The following model descriptions are based on the descriptions included with the software.

MODFLOW is a three-dimensional, finite-difference groundwater flow model designed to simulate aquifer systems that meet the following assumptions:

- saturated-flow conditions exist,
- Darcy's law applies,
- the density of groundwater is constant, and
- the principal directions of horizontal hydraulic conductivity or transmissivity do not vary within the system.

MODFLOW can simulate steady and nonsteady flow in an irregularly shaped flow system. The aquifer layers can be confined, unconfined, or a combination of confined and unconfined. External stresses such as wells, areal recharge, evapotranspiration, drains, and flow through riverbeds can be simulated. Hydraulic conductivities or transmissivities for any layer may differ spatially and be anisotropic, and the storage coefficient may also be spatially varied. A variety of head and flux boundary conditions can be specified. The groundwater flow equation is solved using the finite-difference approximation. The flow region is considered to be subdivided into blocks in which the medium properties are assumed to be uniform. This results in a rectangular grid, which may be variably spaced. The vertical direction zones of varying thickness are transformed into a set of parallel "layers." Several solvers are provided for solving the associated matrix problem. Mass balances are computed for each time step and as a cumulative volume from each source and type of discharge.

Contaminant transport was modeled using MOC3D. MOC3D simulates three-dimensional solute transport of a single reactive species in flowing groundwater. Processes modeled by MOC3D include advective transport, hydrodynamic dispersion (including both mechanical dispersion and diffusion), mixing (or dilution) from fluid sources, and mathematically simple reactions (including linear sorption, which is represented by a retardation factor, and first-order decay). The transport

model is integrated with MODFLOW and uses the method of characteristics to solve the transport equation on the basis of the hydraulic gradients computed with MODFLOW for a given time step. Particle tracking is used to represent advective transport, and explicit finite-difference methods are used to calculate the effects of other processes.

4.1.1 Input data

Hydrological data

The aquifers are considered to be confined systems. Horizons I and II were modeled independently as single layers. The system properties necessary to model groundwater flow in the aquifers include the following:

- Flow conditions in the aquifer (including boundary conditions such as constant head cells, no-flow cells, etc.).
- Starting heads used to initialize the model.
- Either transmissivity or hydraulic conductivity and thickness of the aquifer. The saturated thickness can also be specified for a confined aquifer by providing the top and bottom surfaces of the aquifer.

For Horizon I, the modeled area was expanded from the Phase I analysis to include the region between the fault zone and the Yenisei River. As data for this region are very limited, a hydraulic transmissivity of 2.5 square meters per day (m^2/d) was used for the entire upthrown block (VNIPIPT, 1998). As there were no transmissivity or water head data for Horizon II in this region, the data from the modeled area used in the Phase I analysis was also used in this study. The model grids were evenly spaced, with a 50-m grid spacing along both axes. A mixture of constant head and no-flow cells was used to establish boundary conditions for the model. These boundary conditions are shown in *Figure 4.1*. In general, a constant head boundary was used for the northern and southern boundaries of the systems. No-flow boundaries were used to the east to simulate the wedging out of the horizons.

For modeling in Horizon I, the area under the Yenisei River is modeled as a constant head boundary. In addition, it was found that a proper match between the observed heads and the modeled heads could not be generated unless a section of the Bolshoi Tel was modeled as a constant head zone. The minimum number of constant head cells under the Bolshoi Tel required to match the modeled heads to the observed heads was used. It was found that modeling the section of the Bolshoi Tel to the northeast of the disposal site and a small section to the east of the site as constant head zones reproduced the observed head distribution. In Horizon II, it

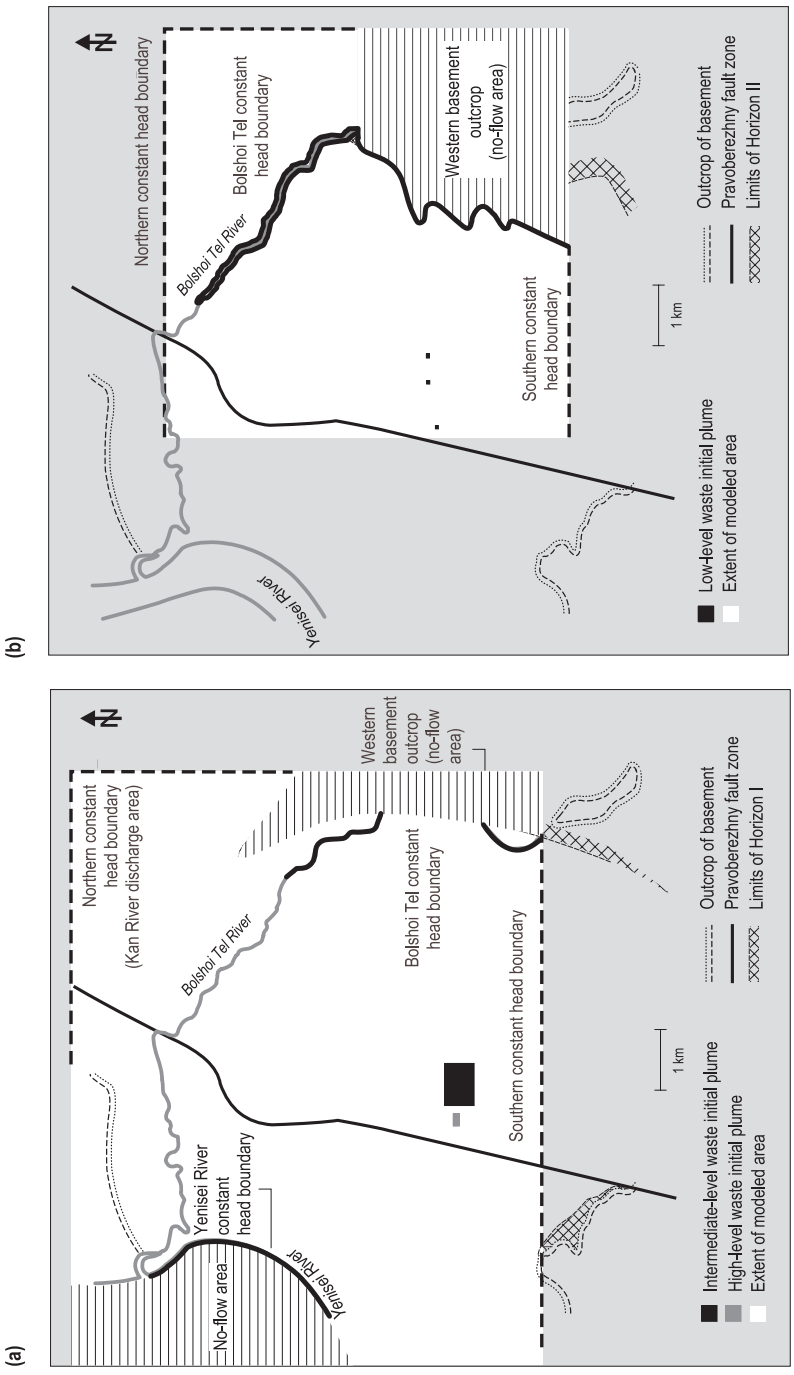

Figure 4.1. Model boundary conditions and initial plume distribution: (a) Horizon I, high- and intermediate-level waste; (b) Horizon II, low-level waste.

was found that the entire area of the Bolshoi Tel had to be modeled as a constant head zone to reproduce the observed heads.

There are two possibilities for modeling the effect of the fault zone. One approach is to assume that the fault zone acts as a perfect barrier to flow and thus use a no-flow boundary. This approach was used in the Phase I analysis, resulting in head errors in the northwestern section of the allotment area. The second approach is to use a very low value of transmissivity for the region of the fault zone, thereby imparting a resistance to flow to match the observed heads. The latter approach was used in this Phase II analysis for modeling in both Horizon I and Horizon II. For Horizon I, the fault zone was modeled as a low-transmissivity area in the region of the disposal site, with a higher value of transmissivity used in the northern section of the fault zone. A more detailed analysis of the approach used to model the effect of the fault zone is given in Chapter 5. For Horizon II, however, there were no data on properties west of the fault zone. In addition, the isopotential lines based on observed heads are perpendicular to the fault zone along its entire length in Horizon II, indicating no-flow conditions. Therefore, a uniformly low value of transmissivity was used to ensure that no flow occurred across the fault zone. Plots of the water heads, hydraulic transmissivity, and basement and roof elevations were provided by VNIPIPT (1998) for each horizon. These paper charts were digitized using Surfer (Golden Software, 1996) and transformed into MODFLOW input files. Some data on the hydraulic properties of these horizons were also provided in tabular format. For further information on the data presented in Chapter 2 of Volume I of this report (Compton *et al*., 2000), see Appendix I.

Waste transport and dose estimation

Modeling the contaminant transport in the aquifers requires additional data. Modeling was conducted for the period following site decommissioning and restoration of normal subsurface flow. MOC3D requires specification of the following data:

- initial contaminant concentration
- aquifer thickness
- aquifer dispersivity
- aquifer porosity
- diffusion coefficient
- first-order (i.e., radioactive) decay coefficient
- retardation factor

Dose analysis was carried out on a unit dose factor basis, with a dose conversion factor (DCF) applied to the concentrations determined by MOC3D. The DCFs used for each radionuclide modeled are given in *Table 4.1*, based on 2.2 L/d

Table 4.1. Radionuclide dose conversion factors.

Radionuclide	Dose factor, Sv/Bq	Dose conversion factor, Sv/yr per Bq/L
^{241}Am	2E-07	1.6E-04
^{135}Cs	2E-09	1.6E-06
^{137}Cs	1.3E-08	1.0E-05
^{237}Np	1.1E-07	9.1E-05
^{239}Pu	2.5E-07	2.0E-04
^{90}Sr	2.8E-08	2.2E-05
^{99}Tc	6.4E-10	5.0E-07

of groundwater consumption. Dose factors are from ICRP Publication 72 (ICRP, 1996).

Contaminants with short half-lives were not modeled in this analysis. Because of the slow rate of groundwater movement in the aquifers, it is expected that institutional controls will be maintained long enough to ensure that these contaminants will decay to permissible levels before reaching the site boundary. For example, tritium, with a 12.3-year half-life, will decay rapidly, dropping approximately three orders of magnitude in 125 years and six orders of magnitude in approximately 250 years.

The consequence analysis of an inadvertent intrusion is highly dependent on the initial contaminant distribution. This is because the maximum dose at any given time in the future corresponds to the maximum concentration at that time, and the maximum concentration at any given time in the future is strongly dependent on the initial contaminant distribution. There are several approaches to determining the initial contaminant distribution. These include explicit modeling of plume formation using a model capable of simulating both hydrodynamic flow and changes in the subsurface chemistry over time; using in situ measurements of the existing contaminant distribution; or making simple assumptions about plume formation.

In the first method, injection operations are modeled explicitly, using data on injection rates and the kinetic properties of geochemical reactions during injection. However, no historical data were available to IIASA on the variation in waste injection rates or the changing composition of the waste stream over time. Moreover, few of the available models can simulate changing geochemical conditions and contaminant transport simultaneously. As the analysis in this report is only a scoping analysis, it was decided to use a simpler, less data-intensive approach.

In the second method, measurements of the plume are taken in situ and the distributions of the plumes are determined using measurements of individual isotopes. Data on the extent of the plume in each horizon were provided by VNIPIPT (1998) and are presented in Volume I of this report (Compton *et al.*, 2000). However, the

boundaries of the plume shown are based on measurements of nonsorbing tritium and nitrate. Since these constituents are not sorbed, they generally will migrate farther during the injection period than contaminants that are sorbed. Use of this plume distribution for sorbed contaminants will thus result in an overestimate of the volume of water contaminated with sorbing contaminants. However, the data available to IIASA only give isotope-specific information on tritium and nitrate levels; other measurements are for gross radioactivity, with no indication of the isotopic distribution in the wells.

This leaves the third alternative, which is to make an assumption regarding the initial plume distribution based on simple models of plume formation. There are two possibilities for a simplified approach. The first is to modify the results of the tritium and nitrate monitoring to account for sorption by reducing the size of the plume for the sorbed isotopes. The second is to set up a plume with a simplified geometry using simple models of plume formation. The latter approach was taken and is discussed in more detail below.

A simple one-dimensional advection dispersion equation for a step input of radioactivity in a constant one-dimensional flow field can be used to model waste injection. This is expressed as

$$\frac{\delta C}{\delta t} = \frac{D\delta^2 C}{R\delta x^2} - \frac{u\delta C}{R\delta x} + \frac{C_{inj} \times u}{R}\delta(x)[h(t) - h(t-T)] \,, \tag{4.1}$$

where C is the aqueous phase concentration; D is the dispersion coefficient; R is the retardation factor; u is the groundwater velocity in the direction of flow; C_{inj} is the activity concentration in the injected fluid; $\delta(x)$ is the delta function; T is the time period of injection; and $h(t)$ is the step function.

Application of this equation requires the assumption that the groundwater velocity, u, is equal to the velocity of the fluid exiting the well screen. As the regional flow field is extremely weak in comparison with the flow field established during injection, this assumption is taken to be valid for the immediate vicinity of the disposal area during the period of waste injection. The plume is formed under the conditions of waste injection and then migrates after site decommissioning under conditions of normal regional groundwater flow. Dispersion is assumed to be negligible. Solution of Equation (4.1) under the stated assumptions shows that the aqueous phase concentration in the aquifer will equal the concentration in the injected waste:

$$C(x,t) = C_{inj}\left[h(x - \frac{u \times t}{R}) - h[x - \frac{u}{R}(t+T)]\right] \,. \tag{4.2}$$

Table 4.2. Estimated plume areas for nonsorbing contaminants.

	Horizon I		Horizon II
	HLW	ILW	LLW
Total volume, m^3	68,000	2,136,000	2,780,000
Effective thickness, m	30	30	30
Porosity	0.07	0.07	0.1
Effective radius, m	102	570	543
Modeled surface area, ha	3.2	102	93

Note: HLW = high-level waste; ILW = intermediate-level waste; LLW = low-level waste.

It can be shown from the solution above that the aqueous volume of a sorbed contaminant is proportional to the inverse of the retardation factor, or

$$V_{aq} = \frac{V_{inj}}{R} , \tag{4.3}$$

where V_{aq} is the volume of contaminated groundwater, V_{inj} is the volume of the injected waste, and R is the retardation factor during injection. The partitioning of the waste between the solid and aqueous phases during injection will therefore result in a reduction in the volume of contaminated water relative to the volume of injected waste while maintaining the injected aqueous phase concentration.

If we assume a constant thickness in the contaminated zone, the area of the plume (and therefore the number of model cells in the layer to be treated as initially contaminated) is directly proportional to the volume of the contamination plume. The properties of the assumed plume for a nonsorbing contaminant are given in *Table 4.2*.

For modeling purposes, the initial concentration was set uniformly at 100 units. In MOC3D, the concentration is given in units of mass per cubic liter (M/L^3). The unit of length in the model is meters; however, the mass units are undefined. Therefore, the units of concentration can be taken as activity per volume, or becquerels per cubic meter (Bq/m^3). Because the plumes were modeled with a uniform concentration of 100 units, the DCFs applied to the model output are given for each waste stream modeled. These are derived using the following formula:

$$DCF_{\text{ingestion}} = \frac{DCF(\frac{\text{Sv/yr}}{\text{Bq/L}}) \times C_{inj}(\text{Bq/L})}{100(\text{unitless concentration})} . \tag{4.4}$$

Multiplying this DCF by the model results gives the dose resulting from ingestion of groundwater at each point in the modeled domain. DCFs for waste streams are given in *Table 4.3* (for high-level waste [HLW] and intermediate-level waste [ILW]) and *Table 4.4* (for low-level waste [LLW]).

Table 4.3. Horizon I transport model isotope-specific parameters.

Radio-nuclide	Injected concentration, Bq/L	Decay constant, 1/d	Modeled retardation factor (*R*)	Dose conversion factor, mSv/yr per 100 units of initial concentration	Estimated plume radius, m
High-level waste					
^{241}Am	7.03E+05	4.4E-06	5	1.1E+03	45
^{135}Cs	1.11E+04	8.3E-10	13	1.8E-01	28
^{137}Cs	2.96E+09	6.3E-05	13	3.1E+05	28
^{237}Np	5.55E+03	8.9E-10	9	5.0E+00	34
^{239}Pu	8.14E+04	7.9E-08	13	1.6E+02	28
^{90}Sr	4.44E+10	6.5E-05	6	9.9E+06	41
^{99}Tc	2.96E+05	8.9E-09	1	1.5E+00	102
Intermediate-level waste					
^{135}Cs	9.19E+03	8.3E-10	30	1.5E-01	68
^{137}Cs	2.27E+09	6.3E-05	30	2.4E+05	68
^{239}Pu	1.35E+05	7.9E-08	200	2.7E+02	26
^{90}Sr	7.55E+07	6.5E-05	26	1.7E+04	73
^{99}Tc	2.96E+05	8.9E-09	1	1.5E+00	373

The HLW and ILW plumes, both located in Horizon I, were modeled separately. The initial plume distributions used for modeling in Horizon I are shown in *Figure 4.1a*. As injection well N-2 is the primary injection well for HLWs, the initial HLW plume was centered on that well. Likewise, the ILW plume was centered on wells N-4, N-5, and N-6. The plots shown are for a nonsorbed contaminant. For sorbing contaminants, the area of the plume was reduced by a factor of $1/R$.

A summary of the isotope-specific input data for modeling waste transport in Horizon I is given in *Table 4.3*.

A value of 1 m was used for the dispersion coefficient in accordance with the estimate of the disperson coefficient from VNIPIPT (1998). A value of 2×10^{-11} square meters per second (m^2/sec) was used for the molecular diffusion coefficient for all contaminants. There were no data on the distribution of porosity in the aquifer. A single value of 0.07 was used for Horizon I, based on Rybalchenko *et al*. (1994). For Horizon I, modeling was carried out for a total of 10,000 years. Outputs were generated for 300, 500, 1,000, 3,000, 5,000, and 10,000 years. The modeled thickness of Horizon I was derived by subtracting the bottom elevation from the top elevation.

Similar assumptions were used for modeling LLW migration in Horizon II. As there were no data on the hydrological properties of Horizon II on the western side of the fault zone, the hydrologic model used in the Phase I analysis was used for the Phase II analysis as well. The initial plume distribution for the LLW in Horizon II is given in *Figure 4.1b*. It should be noted that, as all the modeled constituents of

Table 4.4. Horizon II transport model isotope-specific parameters.

Radio-nuclide	Injected concentration, Bq/L	Decay constant, 1/d	Modeled retardation factor (*R*)	Dose conversion factor, mSv/yr per 100 units of initial concentration	Estimated plume radius, m
^{137}Cs	1.48E+04	6.33E-05	350	1.5E+00	29
^{239}Pu	3.70E+01	7.91E-08	500	7.4E-02	24
^{90}Sr	4.81E+04	6.52E-05	200	1.1E+01	38

LLW in Horizon II are relatively strongly sorbed, the initial plumes used for modeling reflect the reduction in aqueous phase plume area due to sorption. The area occupied by a nonsorbing constituent would be considerably greater, similar to the area shown for the ILW plume in Horizon I. *Table 4.4* gives the model parameters for LLW migration modeling.

Because of the lower amounts of activity and the predominance of short-lived ^{137}Cs and ^{90}Sr in the LLW injected into Horizon II, modeling was only carried out for 1,000 years. Outputs were developed for 300, 500, and 1,000 years. There were no data on the distribution of porosity in the aquifer. A single value of 0.1 was used for Horizon II, based on Rybalchenko *et al*. (1994). As in Horizon I, a value of 1 m was used for the dispersion coefficient and a value of 2×10^{-11} m^2/sec was used for the molecular diffusion coefficient for all contaminants. The modeled thickness of Horizon II was derived by subtracting the bottom elevation from the top elevation.

Geochemical changes in the subsurface

One important factor that was not considered in transport modeling was the possibility of a reduction in the aqueous phase concentration as a result of changes in the geochemical properties in the subsurface. This is of particular importance for the HLWs injected into Horizon I. HLWs are highly acidic saline solutions. The distribution coefficients of the radionuclides are highly dependent upon pH and ionic strength, as shown in *Table 4.5* (adapted from Rybalchenko *et al*., 1994, table 3.8).

During injection, the HLWs are likely to be characterized by distribution coefficients (K_D) similar to those in the pH 2–3 column of *Table 4.5*. These low distribution coefficients are necessary during initial injection to prevent excessive buildup of radionuclides near the screen zone of the injection well, as discussed by Rybalchenko *et al*. (1994). However, after the injection operations, the pH will rise as acids are neutralized, and the ionic strength will fall as the salts migrate away from the radionuclides. The increase in K_D will have two effects in this case. First, the contaminant plumes will move more slowly as the retardation factor increases.

Table 4.5. Dependence of distribution coefficient (K_D) on pH and ionic strength.

pH	2–3[a]	4–5	∼8[b]	8[c]
Ionic strength, μ	1.0	1.0	0.3–0.5	0.1
Radionuclide				
^{90}Sr	1.5–5.5	10–35	7–10	20–30
^{106}Ru	0.5–1.5	7.5–15	2–2.5	4.6–7.5
^{135,137}Cs	1.5–3.0	10–20	8–15	20–50
^{144}Ce	1.0–1.5	40–100	5–10	9.5–19
^{237}Np	(No data)			
^{239}Pu	1.2–1.6	50–120	5–12	15–35
^{241}Am	(No data)			
^{99}Tc	(No data)			

[a]Taken as representative of high-level waste.
[b]Taken as representative of intermediate-level waste.
[c]Taken as representative of normal subsurface conditions.

Second, the aqueous phase concentration will drop as a larger fraction of the radionuclide is transferred to the solid phase while remaining in the same subsurface volume.

The actual distribution of individual isotopes in the subsurface will be governed by a variety of factors. Changes in the distribution coefficient are just one such factor. Because of data and model limitations, detailed analysis of the dynamics of plume formation was not performed. However, any long-term analysis of the repository safety that is sensitive to the maximum contaminant concentration in the subsurface, in either the aqueous or solid phase, will be substantially affected by the initial distribution of radionuclides within the contaminated plume. Better measurements of the isotopic distributions in the plumes would improve this situation. However, the ability to indirectly monitor individual constituents is limited. Transient models to analyze initial plume formation, which incorporate both hydrodynamic and geochemical processes, would be useful in performing a more precise determination of the initial distribution.

4.1.2 Results

The results of hydraulic modeling of Horizon I are shown in *Figure 4.2*, and the results of transport modeling are shown in *Figure 4.3*. The doses from the individual radionuclides in both the HLW and the ILW are summed at each point in the aquifer to give the total dose resulting from all radionuclides at each point in the aquifer. Dose contours are given for 1 millisievert (mSv) in *Figure 4.3a* and for 1 mSv, 10 mSv, 100 mSv, and 1 sievert (Sv) in *Figures 4.3b* and *4.3c*.

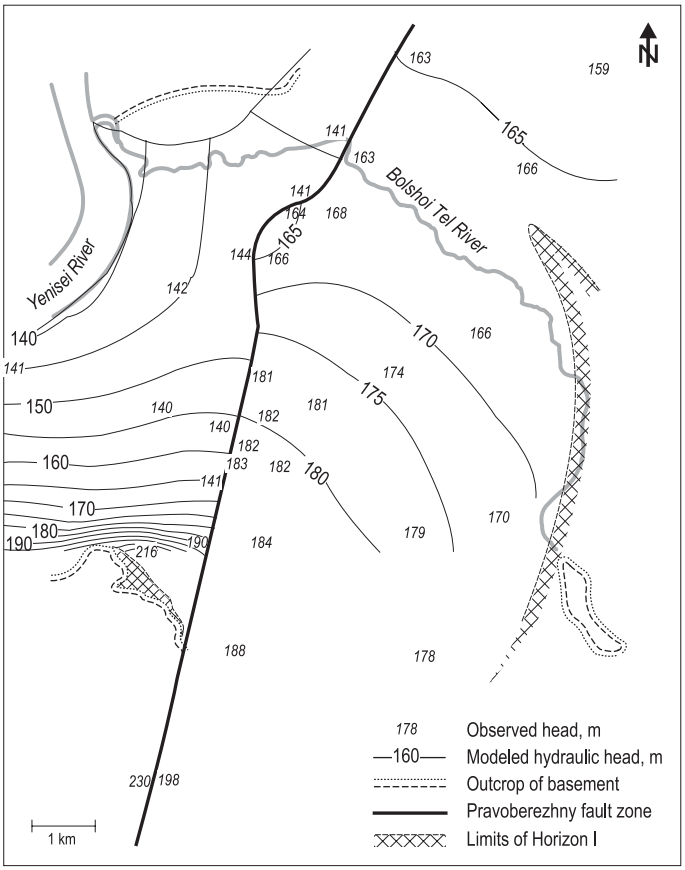

Figure 4.2. Modeled and observed heads in Horizon I.

The resulting picture differs significantly from the picture of waste migration presented in the Phase I analysis. The most obvious difference is the effect of sorption. Apart from ^{99}Tc, which was modeled with a retardation factor of 1 (indicating no sorption), all of the radionuclides migrate extremely slowly. This is true even though the retardation factors used were conservative lower bounds. In reality, the retardation factors are likely to be higher, and thus the plumes are likely to migrate even more slowly. It appears that, because of the very low velocity of groundwater movement, the primary mechanism for dispersal of the wastes will be mechanical dispersion and molecular diffusion. The plumes are almost stationary for relatively strongly sorbed contaminants such as ^{239}Pu, ^{241}Am, ^{135}Cs, ^{137}Cs, and ^{90}Sr; ^{237}Np is somewhat more mobile, but still migrates very slowly. The results of the analysis indicate that these wastes will remain within the current site boundary for at least 10,000 years (the time limit used in this analysis), and in all likelihood much longer.

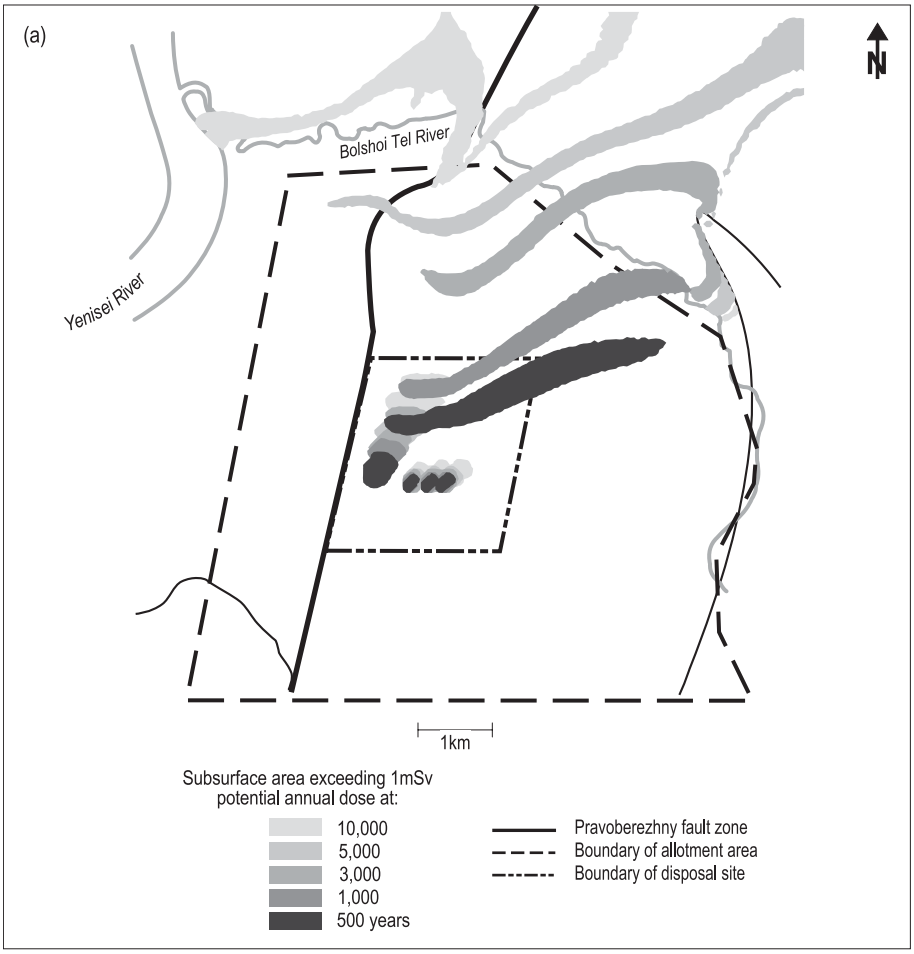

Figure 4.3. Horizon I intrusion doses: (a) from 500 to 10,000 years.

However, due to the extremely slow rate of diffusion, mechanical dispersion, and radioactive decay, high concentrations of long-lived isotopes will also remain.

The maximum doses are shown in *Table 4.6*. The information in this table should be used with caution. Since the dynamics of plume formation were not explicitly modeled, the initial plume concentrations were set equal to injected concentrations on the basis of simple physical considerations. The maximum doses can be quite high, well above the current 1 mSv annual dose limit specified in NRB-96 (1996).

Examination of the ^{99}Tc plume, representative of the migration of a nonsorbing contaminant, shows several interesting features. This plume can be identified in *Figure 4.3a* as the plume that rapidly moves away from the injection site. First,

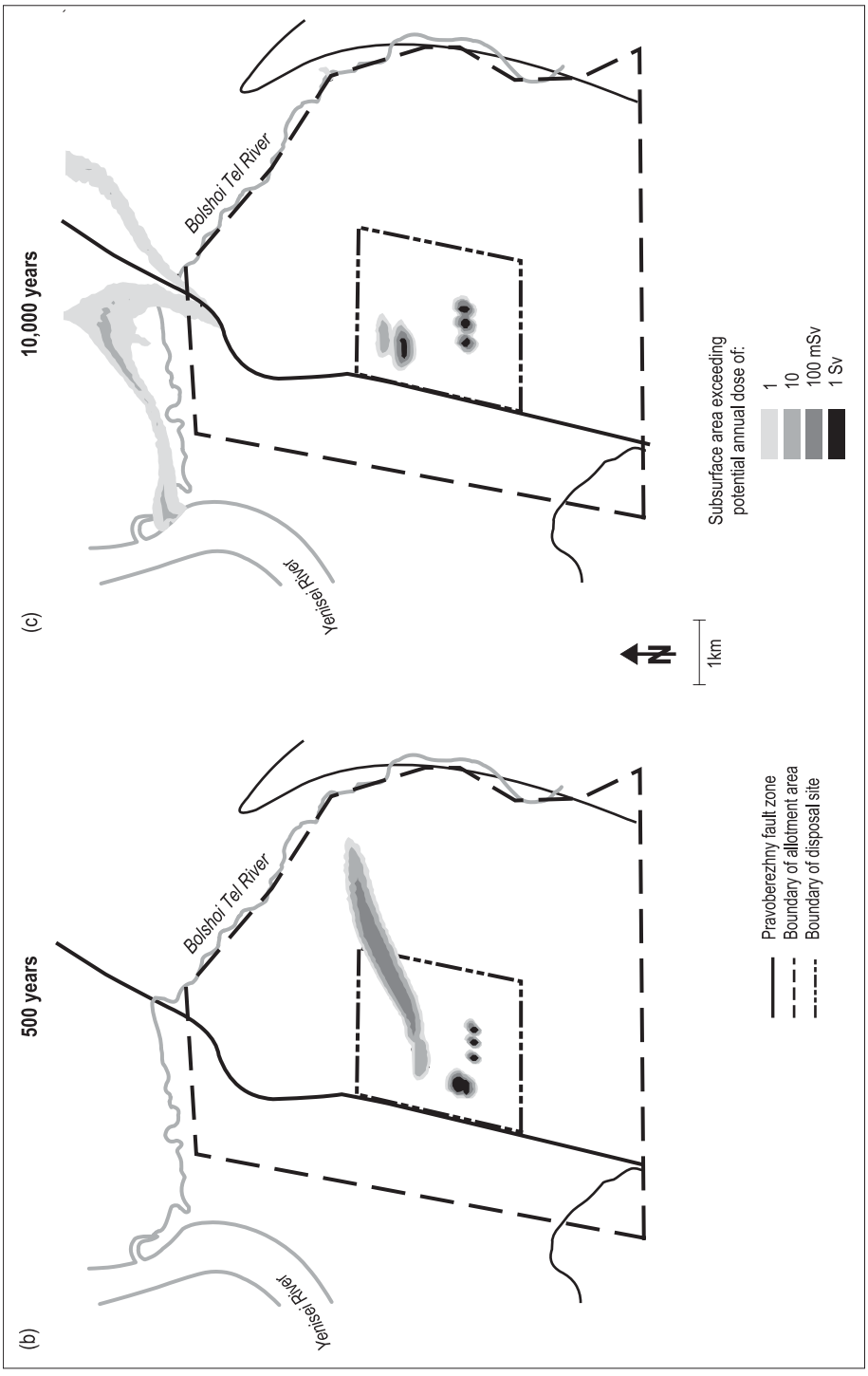

Figure 4.3 (continued). Horizon I intrusion doses: (b) 500 years; (c) 10,000 years.

Table 4.6. Maximum doses from ingestion of water from Horizon I, Sv/yr.

Radio-nuclide	500 years	1,000 years	3,000 years	5,000 years	10,000 years
^{241}Am	5.0E+01	2.2E+01	9.1E-01	3.7E-02	1.2E-05
^{135}Cs	1.8E-02	1.8E-02	1.8E-02	1.8E-02	1.8E-02
^{137}Cs	3.0E-01	2.8E-06	2.4E-26	2.1E-46	1.4E-96
^{237}Np	5.0E-01	5.0E-01	5.0E-01	5.0E-01	5.0E-01
^{239}Pu	2.7E+01	2.6E+01	2.5E+01	2.3E+01	2.0E+01
^{90}Sr	6.7E+00	4.5E-05	9.6E-26	2.0E-46	4.2E-98
^{99}Tc	1.5E-01	1.5E-01	1.5E-01	1.5E-01	1.4E-01

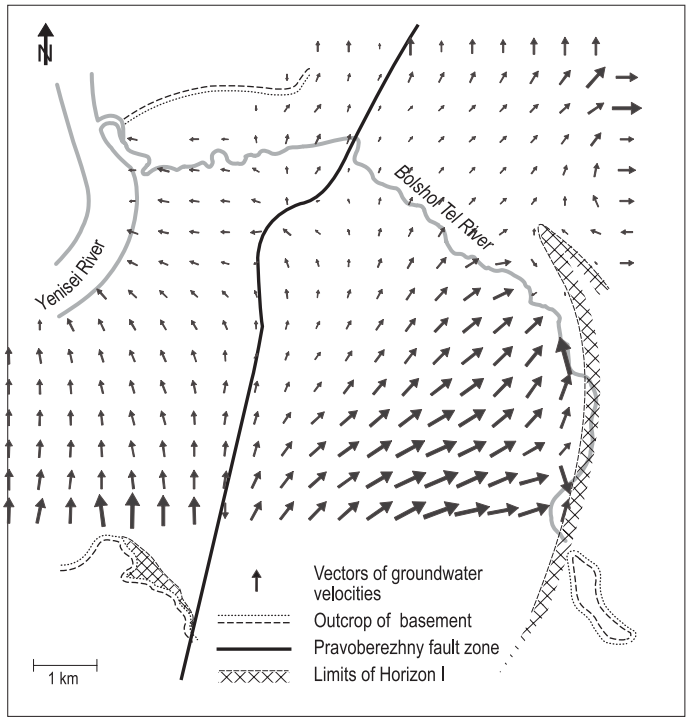

Figure 4.4. Magnitude and direction of groundwater velocity in Horizon I.

the ultimate discharge area of the plume is highly sensitive to the location of the injection well. Waste injected into the eastern wells (primarily ILW) will migrate to the northeast, toward the Bolshoi Tel. Waste injected into the western wells, however, will tend to migrate north and enter the depression north of the injection

site. The divergence of the flow paths can be seen in a vector plot of the magnitude and direction of groundwater velocity, shown in *Figure 4.4*.

Near the eastern end of the injection zone, the groundwater flows fairly rapidly almost due east. Near the western end, the groundwater flows slowly to the north. The capture area of the hypothesized fault zone breach in the northern section of the controlled area can be seen where the velocities curve in to discharge through the fault zone. This can be clearly seen in the plots of migration at 3,000 and 5,000 years in *Figure 4.3a*. At 3,000 years, a slight tail of the plume is captured by the influence zone of the fault zone discharge area and begins migrating westward, toward the fault zone. Between 3,000 and 5,000 years, the plume crosses through the fault zone and enters the upthrown block. Between 5,000 and 10,000 years, the plume begins to contact the hypothesized Yenisei River discharge area. A more complete description of the northern head anomaly is found in Chapter 5.

In addition, the hypothesized area of discharge from Horizon I to Horizon II under the Bolshoi Tel near the northeastern boundary of the controlled area can be seen in *Figure 4.4*. The flow pattern indicates an area of groundwater discharge to the northeast of the disposal site. As the lower boundary of Horizon I is composed of impermeable crystalline rocks, this represents a discharge of waters from Horizon I upward through the confining layer to Horizon II.

The results of waste migration modeling in Horizon II are considerably simpler. The analysis was similar to that conducted in the Phase I report, but was refined by the application of retardation coefficients and radioactive decay for modeling individual plume constituents, providing a more realistic assessment of plume migration. The results of transport analysis are shown in *Figure 4.5*, where the boundary of the contaminated plume is defined as the 1 mSv dose contour.

Because of the much higher level of sorption in Horizon II wastes, the plumes are almost immobile and the short-lived radionuclides ^{90}Sr and ^{137}Cs decay rapidly to below acceptable levels. This can be seen in *Table 4.7*, which shows the maximum doses from ingestion of water from Horizon II.

After 300 years, only ^{239}Pu has the potential to generate doses above the 1 mSv annual dose limit specified in NRB-96 (1996). However, even under the conservative assumption that the initial subsurface maximum concentration is equal to the injected concentration, the annual dose is 7.3 mSv. The area impacted by the ^{239}Pu is expected to be small (see *Figure 4.5*). In addition, if dispersion or geochemical effects during waste injection result in a lowering of the ^{239}Pu aqueous phase concentration in the aquifer below that of the waste as injected, this dose will be lowered and may potentially be reduced to below the 1 mSv annual dose limit specified in NRB-96 (1996).

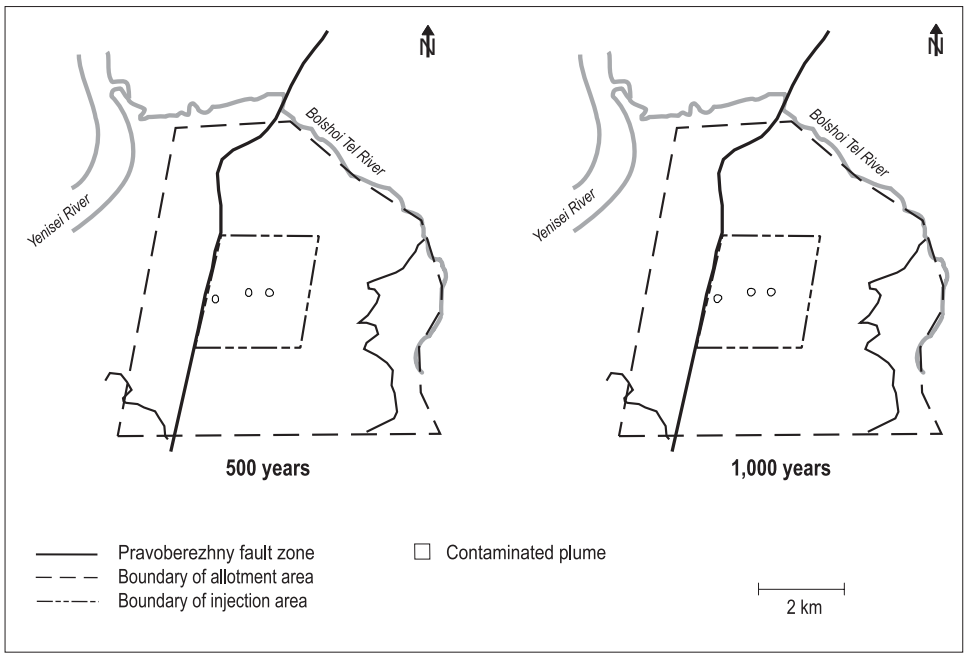

Figure 4.5. Horizon II intrusion doses.

Table 4.7. Maximum doses from ingestion of water from Horizon II, Sv/yr.

Radionuclide	300 years	500 years	1,000 years
^{137}Cs	1.5E-04	1.5E-06	1.4E-11
^{239}Pu	7.3E-03	7.3E-03	7.2E-03
^{90}Sr	8.5E-04	7.2E-06	4.9E-11

4.2 Analysis of Likelihood of Intrusion

A more complete evaluation of the likelihood of an intrusion will be prepared once materials are available. The following factors govern the likelihood of an inadvertent intrusion in the future:

- failure of institutional controls
- groundwater potability
- aquifer yield
- aquifer depth and technical requirements for well placement
- area and location of contaminated plume
- alternative water supplies

Table 4.8. Classification of groundwater based on total dissolved solids content.

Classification	Total dissolved solids, mg/L
Fresh	<1,000
Brackish	1,000–10,000
Saline	10,000–100,000
Brine	> 100,000

Source: Fetter, 1988.

These factors are considered qualitatively in this section using the data that were available to IIASA.

4.2.1 Failure of institutional controls

Institutional controls govern the chance that an individual will be allowed to drill a water well within the restricted area. Institutional controls can be implemented through a number of mechanisms, such as physical security or deed restrictions. The length of time that institutional controls will remain effective is difficult to determine. However, it can be assumed that after 500–1,000 years institutional memory of the site will be lost, and that there will be no administrative control over the territory of the disposal site. The decommissioning plans for the site will presumably address the details of the institutional controls to be implemented, allowing a more complete evaluation of the effectiveness of planned institutional control measures.

4.2.2 Groundwater potability

The second and third factors relate to the attractiveness of the subsurface aquifer as a source of water. The potability of the water is of concern: water that is unfit for consumption based on obvious characteristics such as salinity or turbidity will not be used as a source of drinking water, even in the absence of institutional controls. This is recognized by US regulations on drinking-water wells, in which waters with a salinity greater that 10,000 milligrams per liter (mg/L) are not considered to be viable sources of drinking water (Tsang, 1996). Fetter (1988) lists a classification scheme for water based on total dissolved solids content (*Table 4.8*).

The classification of groundwater based on potential uses is also discussed by Matthess (1982), who examines three use-based classifications: potable water, agricultural water, and industrial water. Groundwater wells for potable water have stringent requirements concerning their physical, chemical, and biological characteristics.

Water intended for agricultural use may have less stringent requirements, depending on the use. Upper limits for total dissolved solids range from 2,860 mg/L for poultry to 12,900 mg/L for fattening lambs. The requirements for irrigation water are generally dependent on the salt-resistance of the crops grown. Water with a sodium chloride (NaCl) content below 500 mg/L is considered always usable for irrigation, whereas water with an NaCl content above 2,000 mg/L is considered only of limited use and water above 4,000 mg/L is considered always unusable.

Water for industrial use has widely varying purity requirements, depending on the use. Waters used in food processing should be at least as pure as potable water. Water used for cooling generally should not be corrosive or contain microbial agents that could cause fouling. The water requirements for steam generation depend primarily on the boiler type. Low-pressure boilers can take waters with up to 700 mg/L, whereas high-pressure boilers generally require waters with less than 0.5 mg/L. Based on these requirements, it appears that, with total salt contents of under 300 mg/L (Rybalchenko *et al.*, 1994), the subsurface waters in Horizons I and II are suitable for potable or agricultural water and may be useful for some industrial uses.

4.2.3 Aquifer yield

The second factor that affects the attractiveness of an aquifer as a source of drinking water is aquifer yield. In the United States, domestic water well requirements can range from 27 to 164 cubic meters per day (m^3/d) (Driscoll, 1986). Wells used strictly for domestic drinking water fall into the lower end of this range; domestic agricultural wells fall into the higher end. Well fields for municipal or industrial uses require considerably more water.

Driscoll (1986) gives rules of thumb regarding aquifer suitability based on transmissivity. Aquifers with a transmissivity greater than 120 m^2/d can be adequate for industrial, municipal, or irrigation purposes, whereas those with a transmissivity less than 12 m^2/d are generally suitable only for domestic wells. Freeze and Cherry (1979) give a value of approximately 1,300 m^2/d as indicative of an aquifer with good possibilities for water extraction. Based on these values and on the values of transmissivity given by Rybalchenko *et al.* (1994) and the data package (VNIPIPT, 1998) of 5–40 m^2/d for Horizon I and 20–80 m^2/d for Horizon II, it appears that the aquifers are only suitable for domestic water well use. Municipal or industrial use, which requires much greater quantities of water, is unlikely for these aquifers.

Table 4.9. Comparison of well-drilling methods.

	Cable tool	Direct rotary
Penetration rate[a]		
Clay and silt	3	5
Loose sand and gravel	2	5
Poorly cemented sandstone	3	4
Well-cemented sandstone	3	3
Usual maximum depth, m	450	450
Maximum feasible depth	90–1,500 m, depending on well bore	–
Equipment	Single-axle truck or trailer	Multiple-axle truck
Comments	Relatively low costs; easily operated; can be operated in inaccessible terrain; requires casing in unconsolidated deposits	High equipment costs; requires experienced personnel; usually requires special drilling fluids

[a] 1 = impossible; 2 = difficult; 3 = slow; 4 = medium; 5 = rapid; and 6 = very rapid.

4.2.4 Aquifer depth and technical requirements for well placement

The fourth factor is the technical requirements for placing a well in the aquifers. There currently are several different methods for drilling water wells. Of the methods currently available, only cable tool drilling and direct rotary drilling are likely to reach the deep aquifers. Other methods, such as driven wells, augured wells, or jetted wells, generally cannot be driven to the depths required to reach the contaminated aquifers. However, it is important to note that these simpler methods may be able to reach the shallow Horizon III, leading to the use of this horizon as a source of groundwater. A comparison of the two relevant methods is given in *Table 4.9*.

Based on the comparison, a cable tool rig is the type of drilling method most likely to be used to reach the contaminated aquifer for a domestic well. However, cable tool drilling to the aquifers would be expensive, and drilling using rotary methods would be even more expensive. These figures indicate that the placement of a water well would require substantial resources, making the aquifers an expensive source of drinking water. However, a simpler variant of cable tool drilling is a hand-operated percussion drill. Such drills have been in use for over 4,000 years and have proved capable of reaching great depths. Hand-operated percussion rigs, constructed from bamboo, were used 4,000 years ago in China to complete wells to depths of up to 915 m (Driscoll, 1986). Such a system, constructed from available materials and operated by the inhabitants, could conceivably reach the

contaminated aquifers. However, it would require enormous effort and is unlikely to be attempted due to the availability of adequate water supplies at much shallower depths.

4.2.5 Area and location of contaminated plume

The area and location of the contaminated plume affect the likelihood of inadvertent intrusion. A contaminated plume extending over several square kilometers is far more likely to be contacted than a plume extending over only a few hundred square meters. In addition, the location of the plume relative to the surface is relevant. Placement of a water well is usually preceded by a surface survey to determine the best chance of finding water. Wells may be more likely to be attempted in valleys than in highlands, as the chance of locating water is generally higher in these areas. This indicates that the area of the injection site would not be considered as favorable a site for a successful water well as the Bolshoi Tel valley or the Yenisei River floodplain. Based on the results of the consequence analysis above, the existing injection field will yield the highest dose due to inadvertent intrusion. However, two factors mitigate this consequence:

- The surface area yielding high doses is very limited. A well would have to be located very close to the existing injection site to contact this plume.
- The area where maximum doses would occur is located close to the regional maximum elevation. Current practice among well contractors would favor a site located closer to the river valleys or floodplains. This may lead to an increase in the significance of the ^{99}Tc plume, which may reach this area.

4.2.6 Alternative water supplies

A major factor in preventing an inadvertent intrusion into the aquifers is the presence of more economically viable water supplies. There are three potential alternate water supplies: water in Horizon III, surface water features, and rainwater.

It has been shown in the consequence analysis that the area of primary concern for intrusion is the area where injection operations are occurring. High levels of sorption will tend to immobilize the most significant contaminants, ^{239}Pu and ^{241}Am. Because of the high degree of sorption and the very low groundwater migration rate, these contaminants will move only a short distance even over thousands of years. Therefore, the presence of adequate quantities of good-quality groundwater overlying these areas will minimize the chance that a prospective domestic well driller would continue to sink a shaft below a viable source of drinking water. Horizon III is present above the injection site as a relatively homogeneous

Table 4.10. Annual average precipitation (mm) and temperature (°C) in the Zheleznogorsk region.

	Jan	Feb	Mar	Apr	May	Jun	July	Aug	Sep	Oct	Nov	Dec	Annual
Temperature	–18.3	–15.9	–7.9	1.7	9.1	16.4	19.4	16.2	9.6	1.6	–9.1	–16.6	0.5
Precipitation	15	12	15	27	43	57	84	76	51	41	34	24	479
Water supply rate[a]	5	4	5	9	14	19	28	25	17	13	11	8	13

[a]Liters per day, based on a 10 m^2 catchment area.

sandy layer ∼20–50 m thick, at a depth of ∼60 m. Although data on the geohydrology of this horizon were not available, it seems reasonable to assume that this layer is saturated and that the hydraulic conductivity is at least as high as that of the deeper aquifers. For purposes of a domestic well, this aquifer seems to be quite adequate. In addition, the much shallower depth would make this aquifer reasonably accessible using most simple drilling methods.

Another potential alternate water supply is surface water. However, no significant surface water features are indicated in the area of the injection site. The distance to flowing surface water, either the Yenisei or the Bolshoi Tel, is several kilometers. The use of river water in the area of the site would thus require a piped water system and, given the potential for pollution of surface water, may not be attractive.

The final alternate water supply is rainwater. The annual average precipitation is given in *Table 4.10*. Depending on the catchment area of a cistern and the water supply needs of a household, precipitation may be adequate to provide water during the summer and autumn months. Precipitation during the winter is relatively low, however, and combined with the very low temperatures during this time, it would be quite difficult to keep a water system free of ice. A water tank buried below the freeze line would be necessary to provide a year-round water supply based on precipitation. Rain-based water supplies therefore do not seem to be a viable year-round water supply solution for a residence near the injection site.

Based on a brief overview of alternate water supplies, the most likely source of water for a residence or small community in the region of the injection area is groundwater from Horizon III or a shallower water-table aquifer. This indicates the need to prevent the introduction of contamination into Horizon III from the deeper disposal horizons. Fortunately, the likelihood of contamination from Horizon I is low at the disposal site because of the head difference between Horizons I and II in these areas. If a breach were to occur in the confining layers between Horizons I and II, the difference in water heads would cause downward water flow from Horizon II to Horizon I. However, information on the head levels in Horizon III is not available to IIASA. If the head levels are lower than in the deeper aquifers,

a rupture in the confining layer between Horizon II and Horizon III may lead to upward water flow and subsequent contamination of Horizon III. The most likely cause of such a disruption would be a failure of the existing wells that penetrate these layers. Such a failure could be of two types: either a failure of the grouting between the formation and the casing string, which would lead to communication between adjacent aquifers along the outside of the casing string; or a breach of the grouting and casing string in the saturated zones, leading to a potential for communication between aquifers through the interior of the casing string. The likelihood of either type of breach is dependent on the method and quality of the decommissioning of the inactive wells after site shutdown. This may be analyzed in more detail when the decommissioning plans of the site are known.

VNIPIPT (1998) divides the potential users of the groundwater at the site into two groups: low-capacity users, such as domestic water supply wells for individual households or small settlements; and high-capacity users, such as municipal water wells. Low-capacity users could be expected to use, at most, up to only a few hundred cubic meters per day. Municipal water supplies, on the other hand, would require yields of over 50,000 m^3/d. The groundwater resources at the site can be divided into two groups: relatively shallow aquifers and deep aquifers. The shallow aquifers include unconfined aquifers in the Quaternary sediments, aquifers in the valleys of the Yenisei and Bolshoi Tel Rivers, and the confined aquifer in Horizon III. These aquifers lie at depths of tens of meters to less than 100 meters below ground. The deep aquifers include Horizons I and II, lying at depths greater than 100 meters below the surface. Because of the synclinal nature of the formation, in the injection area Horizon III lies approximately 90 m above Horizon II, and Horizon II lies approximately 205 m above Horizon I.

Low-capacity users would be expected to use only the shallow aquifers. It is likely that adequate fresh water would be encountered in the shallow Quaternary deposits and no attempt would be made to reach the deeper disposal horizons. Prevention of contamination of these overlying aquifers is important in preventing unacceptable doses to future occupants of the site.

High-capacity municipal users, on the other hand, would be expected to use the waters in the sediments under the the Bolshoi Tel or Yenisei Rivers. This is consistent with the experiences at Seversk (Tomsk-7) and Zheleznogorsk (Krasnoyarsk-26), where municipal water supplies are located in sedimentary deposits under rivers, rather than in deep aquifers. In addition, the yield from the disposal aquifers is expected to be too low for use as municipal water supplies. It was estimated by VNIPIPT (1999) that extraction of 50,000 m^3/d would consume all sources of recharge in Horizon I and would require a network of over 100 wells, each operating at the maximum sustainable Horizon I extraction rate of approximately 500 m^3/d (see *Table 5.1* for results from pumping tests). Because typical extraction

Table 4.11. Water supplied from water wells.

Type of water supply	Per capita water consumption rate, m^3/d	Number of people supplied by well producing: 180 m^3/d	500 m^3/d
Domestic user, small rural settlement	~0.06	3,000	8,300
Centralized water supply, large rural settlement	0.12–0.16	1,100–1,500	3,100–4,200
Centralized water and heat supply, urban settlement	0.23–0.35	500–780	1,400–2,200
Centralized water and heat supply, major city	0.4–0.6	300–450	800–1,300

Table 4.12. Cost of well completion.

Depth	Cost, 1,000 US dollars
Less than 100 m	2–4
~350 m	30
800 m	550
1,500 m	1,000

Table 4.13. Per capita cost of well completion.

	Per capita cost (US$) for 180 m^3/d well completed to: 350 m	550 m
Centralized water supply, large rural settlement	20–27	370–490
Centralized water and heat supply, urban settlement	38–58	700–1,100
Centralized water and heat supply, major city	67–100	1,200–1,800

rates are lower (approximately 180 m^3/d), it is more likely that over 300 wells would be required.

For purposes of evaluation, *Table 4.11* indicates the per capita water use in the Russian Federation (VNIPIPT, 1999) and the number of people served by a well operating at typical (180 m^3/d) and maximum (500 m^3/d) extraction rates. In addition, *Table 4.12* presents the data available on the cost of well completion to different depths (VNIPIPT, 1999). Using the figures for a well producing 180 m^3/d and the figures for the per capita consumption rate, we can see that the per capita cost of a well supplying a centralized water system would be as given in *Table 4.13*.

Based on these figures, it appears that individual households would be deterred from completing a well by the high costs associated with the well and the inability to spread the costs of well construction over many people. The large-capacity

users, such as a major city, would be more likely to be deterred by the inability to produce adequate amounts of water. However, a single well or a pair of wells could supply a large rural settlement of several thousand households with a water supply at a cost for well construction ranging from tens to hundreds of dollars per household. Although this may be an expensive source of water, it is not out of the reach of such a settlement. If alternate water supplies are not available, it could be economically feasible to draw water from at least the upper Horizon II, if not the shallower sections of Horizon I. It should be noted that surface waters and shallow aquifers may be subject to other sources of pollution, such as improper waste disposal techniques or pollution from agricultural sources. Deep aquifers are therefore sometimes considered attractive because of their potential to offer clean water supplies, unaffected by surface contamination conditions. This again points to the need for the protection of the overlying aquifers as a protective buffer against intrusion into the deeper disposal horizons.

The mobility of ^{99}Tc may pose some problems, as this radionuclide may reach the discharge area of the aquifer with subsurface concentrations in Horizon I, resulting in doses well above 1 mSv per year. However, the plume would have to migrate vertically through the confining layers of Horizons I and II to affect the areas most likely to be used for drinking-water supplies. The combination of horizontal and vertical travel time indicates that this is a problem that would occur only after thousands of years. The seepage of this contaminant from the underlying layers would be mixed with the flow through the aquifer in which the well is located. It is not possible to judge the significance of this pathway as no data were available for modeling waste flow in Horizon III or the sub-riverbed aquifer. Data on the hydraulic properties of the overlying aquifers and the interactions of the rivers (Bolshoi Tel, Kan, and Yenisei) with the groundwater at the site would allow a better understanding of potential consequences of ^{99}Tc migration.

4.2.7 Summary

Water use from Horizons I and II cannot be ruled out on the basis of the existing data concerning potability. The groundwater at these horizons appears to be of sufficient quality for almost any use. However, we can see that the use of these aquifers as a high-capacity municipal or industrial water source is likely to be ruled out by the low transmissivity of the aquifers. Two factors reduce the likelihood that the aquifers will be used for a domestic well. The first is the depth to the groundwater. Although these aquifers are within the reach of any reasonably foreseeable technology, drilling such a well would require an enormous effort. It appears unlikely that this level of effort would be undertaken by a domestic user. The other factor is the presence of the overlying Horizon III, which is more likely to be exploited by a domestic user than the deeper horizons. Although data were not available to

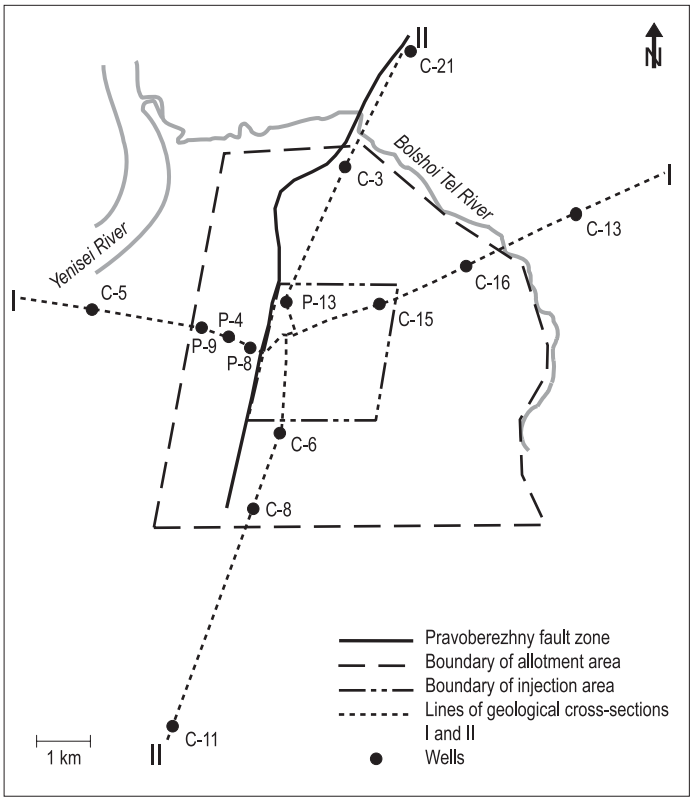

Figure 4.6. Disposal zone and exclusion zone at the Severny site.

evaluate the attractiveness of Horizon III as a water supply, it seems reasonable to assume that this aquifer would be exploited before a water well would be sunk into the deeper horizons.

Concern about the doses calculated in this analysis must be tempered by the recognition that risk is a function of both hazard and exposure. If there is no exposure, there is no risk, even if the potential hazard is high. Several factors influence the likelihood of an inadvertent intrusion into the disposal horizons, and hence the likelihood of exposure to the waste. The first factor is the effectiveness of the institutional controls in preventing placement of a drinking-water well. As discussed by Rybalchenko *et al*. (1994) and by VNIPIPT (1999), the area of the site is subject to strict controls. Use of groundwater inside the disposal zone is prohibited. Use of waters outside the disposal zone, but within the exclusion zone, is only allowed in coordination with supervisory bodies. The location of these zones is shown in *Figure 4.6*.

It can be reasonably assumed that exposure via the drinking-water pathway will not occur while institutional controls are effective. However, it can be expected that, after some time, institutional knowledge of the existence and hazards of the disposal site will be lost. Although it is not possible to predict exactly when this will occur, it is reasonable to assume that it will occur within 500–1,000 years. After this time, the likelihood of exposure will be governed by the the attractiveness of the aquifers as a drinking-water supply. The subsurface waters at the site appear to be fresh waters, with total salt contents under 300 mg/L. Although detailed chemical analysis of the subsurface waters was not available, the extracted groundwater can be considered potable water on the basis of the total salt content. Therefore, the primary protective factors are the depth to the disposal aquifers and the yield of the aquifers, coupled with the availability of alternate drinking-water supplies.

In summary, it appears that although the consequences of intrusion into the deep aquifers could be severe, the likelihood of such intrusion is very low due to the depth to the waste, the low yield of the aquifers, and the presence of more favorable water supplies either in the shallow sedimentary deposits or in the sediments under the Yenisei and Bolshoi Tel Rivers. The consequences of the high mobility of ^{99}Tc are not clear but would be clarified by an examination of the dynamics of the discharge areas of the disposal horizons and the overlying aquifers.

4.3 Conclusions

High subsurface concentrations of long-lived transuranic radionuclides will remain in the Horizon I groundwater within the current site boundaries for tens of thousands of years. These plumes will generally be limited in area and will migrate extremely slowly, dissipating their concentrations through dispersion, diffusion, and radioactive decay. Of all the long-lived radionuclides, only ^{99}Tc will migrate outside the site boundary in the next 10,000 years, reaching the northeastern site boundary in approximately 1,000 years, passing through the fault zone north of the site sometime between 3,000 and 5,000 years, and reaching the Yenisei River discharge area in 5,000 to 10,000 years. If intrusion into the contaminated plume were to occur, doses several orders of magnitude above the allowable level would occur. The transuranic plumes, representing the most hazardous areas, are of limited extent. Intrusion into the peak of a transuranic plume and subsequent use of the contaminated water as drinking water could lead to annual doses of over 1 Sv, with ^{241}Am and ^{239}Pu contributing most of the dose. The ^{99}Tc plume, representing a substantially lower but still significant dose, is likely to disperse over a wide area, with part of the plume discharging upward into Horizon II after thousands of years, part discharging through the disturbance in the fault zone north of the site, and the remainder continuing to migrate northward toward the Kan River. Intrusion into

this more mobile plume and exploitation of the groundwater could result in annual doses of up to 150 mSv.

In Horizon II, higher levels of sorption should retain the major radionuclides (^{90}Sr, ^{137}Cs, and ^{239}Pu) within the disposal area. Radioactive decay will reduce the drinking-water dose from ^{90}Sr and ^{137}Cs to below permissible levels in less than 300 years. The conservative analysis conducted here indicates that ^{239}Pu will remain at levels that could generate an annual dose of approximately 7.3 mSv.

However, several factors reduce the seriousness of the high doses determined in the consequence analysis. The most important is the probability of exposure. Based on a qualitative examination of the likelihood of groundwater intrusion into Horizon I, there is very little chance that the high doses calculated in the consequence analysis will actually be received. Although it is not possible to give a quantitative estimate of this probability, the depth to the groundwater in Horizon I (and resulting costs and effort to place a well) indicates a low probability of exposure, particularly since there is more accessible water in Horizon III.

A second factor that must be considered in evaluating the significance of the consequence analysis is the highly conservative nature of the analysis. The maximum concentrations in the subsurface were assumed to be the same as the concentration in the injected waste. The initial distribution of long-lived radionuclides in the subsurface, in both the solid and aqueous phases, will determine the potential doses for tens of thousands of years. This is because the plumes tend to maintain their geometry under conditions of regional flow, slowly being advected away from the disposal zone. Unfortunately, detailed data required to accurately model the near-field problem were not available. On the positive side, however, the data required to perform this analysis appear to exist within the responsible institutions in Russia. In addition, if the plumes retain their geometry after injection ceases, a great deal of insight may be gained from more detailed monitoring of individual constituents during the decommissioning process. The reliance on modeling may be considerably reduced by direct measurements of the aqueous phase concentration of long-lived radionuclides in the aquifer.

5
Failure of the Pravoberezhny Fault Zone

The area of waste disposal is displaced vertically in relation to the Yenisei River. In the area of the disposal site, the sedimentary strata of Horizon I are in direct contact with the crystalline rocks of the upthrown block with a displacement between the blocks of between 250 m and 270 m. This leads to a relatively impermeable boundary between the disposal area and the Yenisei River. However, a failure of this fault, either at the disposal area or within the area of influence of the disposed wastes, could lead to waste migration toward the Yenisei River. A failure of the fault zone that results in the creation of a flow window toward the Yenisei and consequent discharge of contaminated groundwater into the Yenisei River was therefore evaluated. Studies related to a failure of the fault zone were carried out by IIASA, IGEM, and VNIPIPT. VNIPIPT (1999) provided additional data and analyses to support their assertion that the fault zone acts as a confining layer, limiting migration toward the Yenisei River. IGEM (1999b) provided an analysis of the potential failure modes of the fault zone, including the type and location of failure. IIASA conducted an analysis of the changes in groundwater flow patterns and the potential for contamination of the Yenisei River due to a failure of the fault zone.

5.1 Analysis of Fault Zone Geology near Deep Storage for Liquid Radioactive Waste at the Mining and Chemical Combine

A great deal of work has been carried out to evaluate the geology of the fault zone and the role that it plays in preventing waste transport toward the Yenisei River. The importance of the fault zone was recognized early in the process of designing the repository. It was first studied intensively by a team of geologists from the Krasnoyarsk Territorial Geological Administration in 1958. Since then, a variety of studies have been performed to extend knowledge of the area. These range from pumping tests and geophysical surveys carried out in the 1960s (Goncharov and Nosukhin, 1963, 1965; Goncharov and Krivocheev, 1966, 1967) to more recent

evaluations of the tectonic characteristics of the region of the disposal area (Lukina, 1994, 1996; Kupalov-Yaropolk *et al*., 1997).

5.1.1 The Pravoberezhny fault as a barrier to flow: A review of the evidence

VNIPIPT provided evidence of the isolating properties of the fault zone under current conditions. Some of the strongest evidence of the effectiveness of the fault zone in limiting flow to the west is the difference in static water levels across the fault zone and the distribution of heads in the downthrown block. The gradient of hydraulic head near the fault zone is roughly north–northeast, or parallel to the plane of the fault zone, as can be seen in *Figure 5.1*. This figure represents the head pattern based on the calculations of VNIPIPT, as provided in the Phase I study (VNIPIPT, 1998). This flow pattern, coupled with the difference in water heads across the fault zone, indicates that the direction of flow in the disposal area is to the north and east, rather than to the west across the fault zone.

In addition, pumping tests and geophysical surveys carried out prior to disposal operations recorded a significant barrier to flow across the fault zone (Goncharov and Nosukhin, 1965). A series of paired wells, one on either side of the fault zone, was placed along the length of the fault zone, extending from wells C-46 and C-31, located 5–6 km south of the injection array, to wells C-37 and C-33, located 4–5 km north of the injection array. Pumping tests were conducted to determine the potential for groundwater flow across the fault zone. It was found that pumping of the wells on one side of the fault zone did not influence water levels on the opposite side of the fault. *Table 5.1* provides the results of pumping tests conducted in wells located across the fault zone; water levels in observation wells did not change in any of the pumping tests shown in *Table 5.1*. The lack of water level change in wells located on the opposite side of the fault zone can be interpreted as evidence of the impermeability of the fault zone in the disposal region. This was taken as evidence for the confining ability of the fault.

Finally, operational records from the site showing water level variations during injection observations show no changes in water levels of wells in the upthrown block, even though relatively high injection rates ($\sim$300 m^3/d in Horizon I and $\sim$600 m^3/d in Horizon II) are maintained throughout much of the year. *Figure 5.2* shows the head contours in the disposal area during injection. These provide strong evidence that the fault zone serves as a barrier to flow for the contaminated groundwater. These observations, coupled with the relative difference in static water heads in wells across the fault zone ($\sim$40 m in the area of the disposal site) and the isopotential lines constructed from the pre-injection water levels in wells distributed across the site, all point to the role of the fault zone in confining the contaminated waters of the disposal area from the Yenisei River. The perpendicularity of

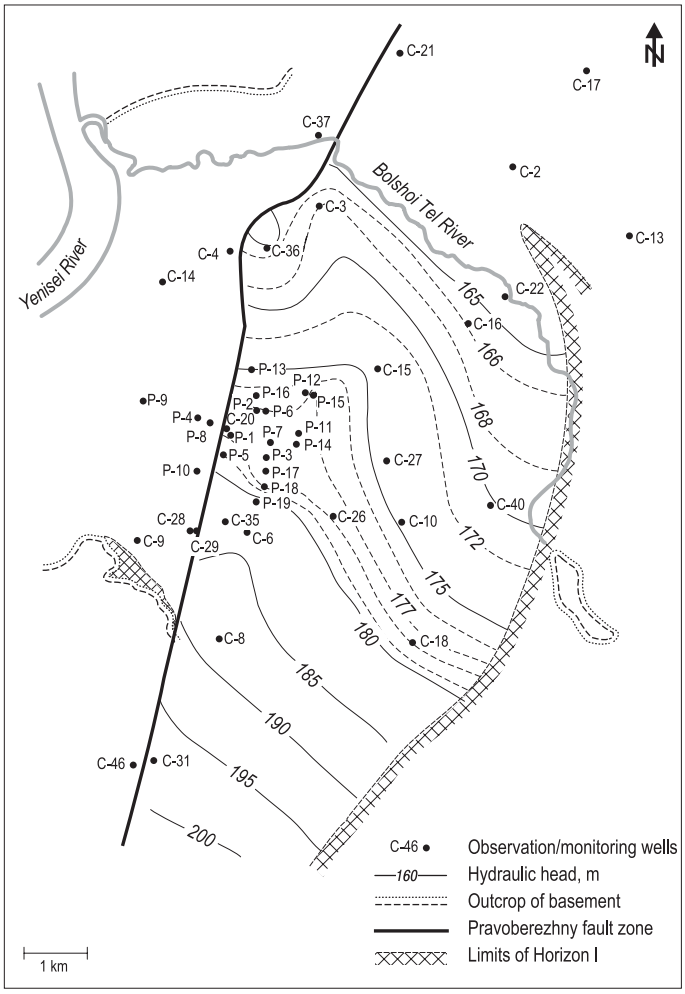

Figure 5.1. Hydraulic head distribution in Horizon I.

the isopotential lines to the fault zone in the region of waste disposal is indicative of a no-flow barrier.

However, there is more ambiguity several kilometers to the north of the fault zone, as can be seen in the water levels of wells C-4 and C-36. In well C-36, the water head is 165.25 m; in the conjugate well C-4 of the upthrown block, the water head is 143.17 m. This represents an anomaly if the water heads in the downthrown block are correct, as the water level in well C-36 should be approximately 173 m if a no-flow boundary is present in this region. In addition, the head in well C-38 (163.7 m) is approximately 4 m lower than the head in well C-3 (167.78 m) (see *Figure 5.5a*). The distance between these wells is only approximately 250 m,

Table 5.1. Pumping tests across the Pravoberezhny fault zone.

							Information on observation wells		
Well	Horizon	Pumping time, hours	Discharge, L/sec	Drawdown, m	Specific well discharge, L/sec/m	Transmissivity, m^2/d	Well	Horizon	Distance from pumping well, m
C-30	II downthrown block	238	1.85	47.0	0.04	8.3	C-46	Upthrown block crystalline basement	280
C-31	I downthrown block	184	6.0	59.0	0.1	4.0	C-31	I downthrown	320
							C-46	Upthrown block crystalline basement	
C-35	I downthrown block	169	1.2	185.0	0.006	1.2	C-30	II downthrown block	320
							C-28	I upthrown block	400
							C-29	I upthrown block	250
C-36	I downthrown block	299	1.3	74.7	0.017	1.3	C-4	I upthrown block	480
							C-3	II downthrown block	1010
P-5	I downthrown block	76	1.0	86.9	0.011	0.9	P-8	I upthrown block	430
C-20	II downthrown block	124	1.45	60.2	0.024	4.8	P-8	I upthrown block	230
P-8	I upthrown block	212	0.54	18.6	0.029	9.0	C-1	II downthrown block	370

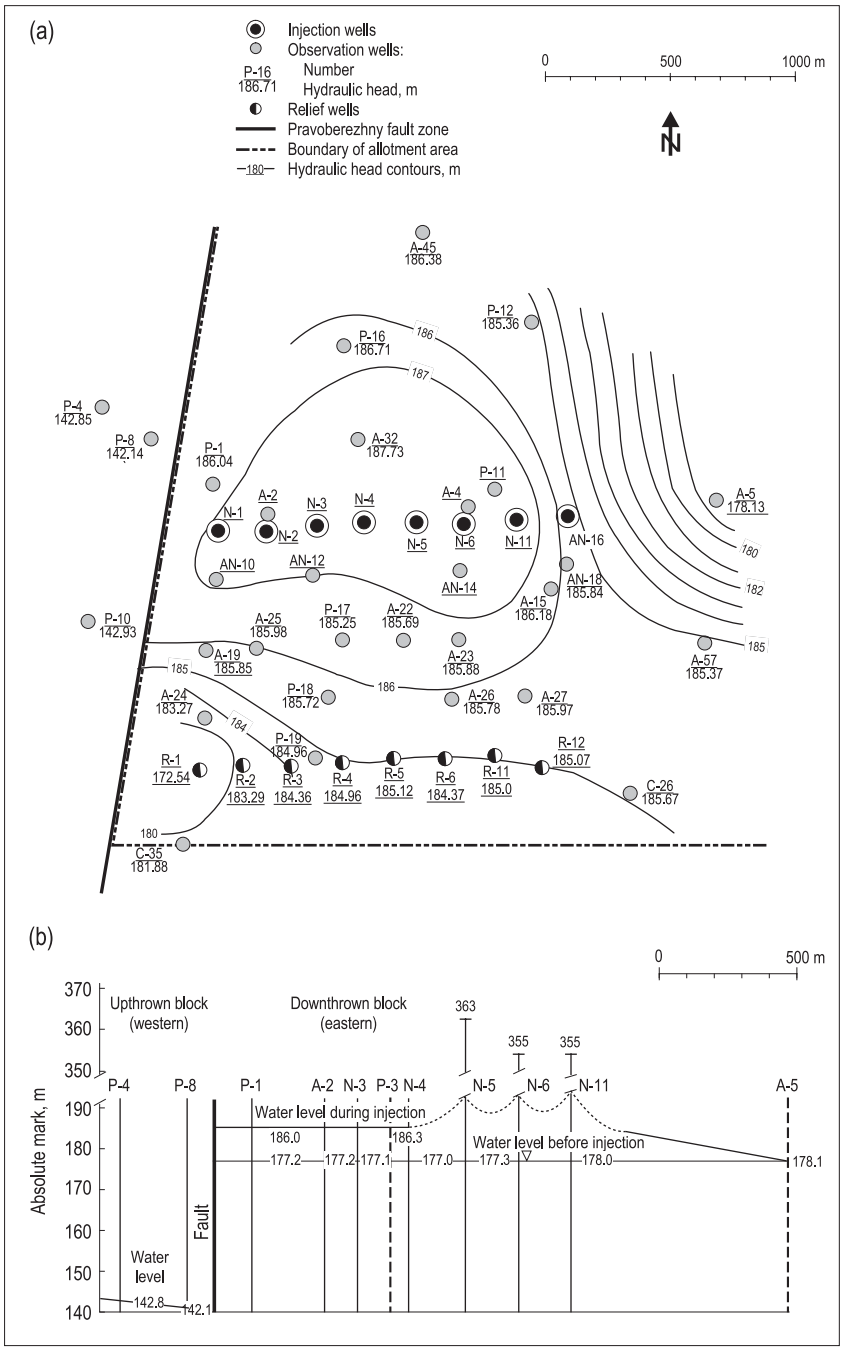

Figure 5.2. Hydraulic heads in the disposal area during injection operations: (a) plan view; (b) cross-section through fault zone.

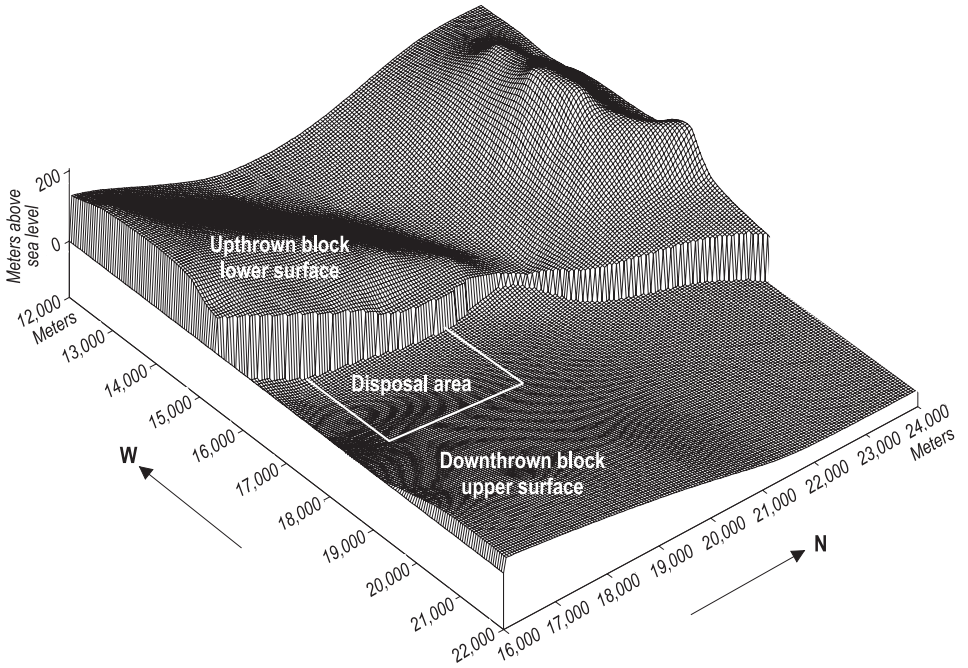

Figure 5.3. Difference in elevations between the upthrown and downthrown blocks.

indicating a gradient toward the fault zone perpendicular to the gradient leading to the Kan River.

Another piece of evidence for the gradual weakening of the confining ability of the fault zone as it is traversed to the north is the difference in the elevation of the upper boundary of Horizon I in the downthrown block and the elevation of the basement rocks in the upthrown block. A plot of elevations was derived from contours of the upper and lower surfaces of Horizon I provided by VNIPIPT (VNIPIPT, 1998) and is shown in *Figure 5.3*. The figure is a plot of the upper surface of the downthrown block (in the east) and the lower surface of the upthrown block (in the west). Care should be taken in interpretating this figure, as the elevation of the layers near the fault zone is determined by extrapolation from more distant measurements. In particular, this plot does not account for deformation of the layers due to past vertical movement of the fault, and it shows an increase in separation to the far north of the site (north of the Bolshoi Tel) that is likely an artifact of extrapolation. However, it does yield a picture of the trend in the separation of the two blocks. It can be seen from the figure that this degree of separation is relatively high in the neighborhood of the disposal area (over 150 m). In the region of the fault zone bend, this difference drops dramatically. It is clear that in an area where the

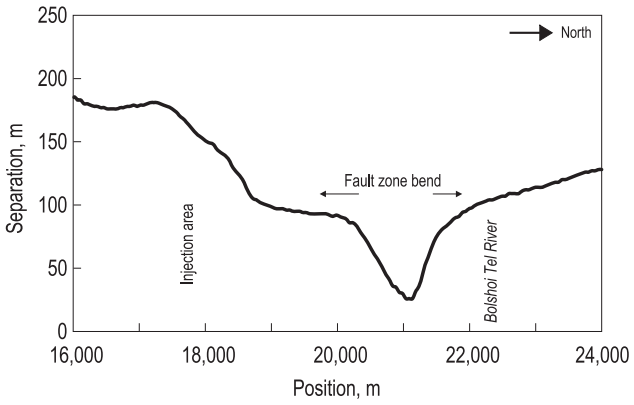

Figure 5.4. Separation of upthrown Horizon I basement and downthrown Horizon I roof.

elevation of the upper surface of the downthrown block is higher than the elevation of the lower surface of the upthrown block, there is a potential for the two sections to be in hydraulic communication across the fault zone. According to this plot, the difference in these two elevations (upthrown basement elevation–downthrown roof elevation) is greater than zero along the entire length of the fault zone. However, there is a sharp plunge in the difference between these elevations in the area of the fault zone bend. This can be seen more clearly in *Figure 5.4*. It is interesting to note that this sudden plunge in the difference in elevations corresponds to the location of the anomalous well heads in wells C-4 and C-36 (see *Figure 5.1*).

Cross-sections of the fault zone in this region confirm this decrease in the amplitude of the fault zone displacement north of the disposal ground. This can be seen more clearly in the cross-section of the fault zone between wells C-3 (downthrown) and C-39 (upthrown) (*Figure 5.5a*). These wells are located to the north of the area of the fault zone bend. Finally, continuing to the north, the cross-section between wells C-33 and C-37 (*Figure 5.5b*) shows an area where the sands and sandstones of the downthrown Horizon I are in direct contact with the sedimentary deposits of the upthrown block, rather than in contact with the crystalline basement rock.

The large elevation difference in the two blocks near the injection wells, the lack of a plausible mechanism of fault zone failure in this area, and the difference in static and dynamic water heads in the region all point to the likelihood that the fault zone is and will remain an effective barrier in the vicinity of the disposal area. The evidence points to the region north of the disposal area, either in the bend of the fault zone or slightly north of it, as the most likely area for a disruption in the

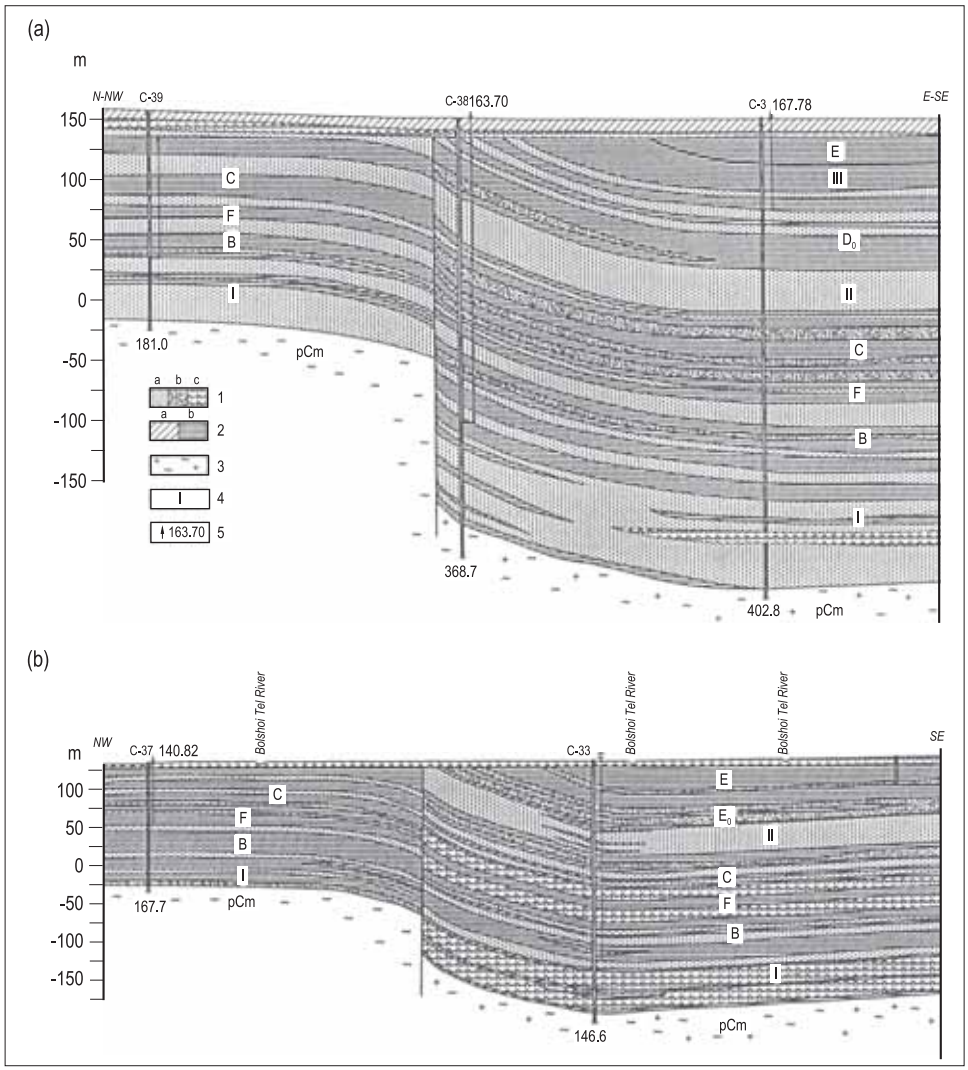

Figure 5.5. Geologic sections: (a) line connecting wells C-39 and C-3; (b) line connecting wells C-37 and C-33. (1) Permeable rocks: sands (a), sandstones (b), and gravel sands (c); (2) impermeable rocks: Quaternary sediments (a) and clays (b); (3) basement rocks; (4) symbols for horizons; (5) altitudes of groundwater heads in meters.

fault zone and a flow window toward the Yenisei River. This conclusion is also supported by tectonic evidence and is discussed in the section below.

5.1.2 Disjunctive tectonics of the Yenisei–Kan interfluvial area

The tectonic characteristics of the disposal region were examined by IGEM (1999b) to evaluate the potential failure modes of the fault zone. Their report forms the basis of this section. To evaluate the potential for adverse seismic activity at the site, a general overview of published and archived geologic–geophysical materials characterizing the composition and development history of the investigated region are discussed below.

The Yenisei–Kan interfluvial area is located near the conjunction of the three largest geotectonic elements of the Asian continent: the ancient Siberian platform, the epi-Paleozoic West Siberian plate, and the Altai–Sayan orogenic area. The general geological characteristics of this area are given in *Figure 5.6*. The interfluvial region is separated from these three geotectonic units by regional fault zones: from the northwest by the Yenisei fault, from the south by the Iisk–Kan fault, and from the east by the Kan–Yenisei fault. The interfluvial region lies between the Siberian platform (absolute elevations from 90–120 m up to 370 m) and the northwestern spurs of Altai–Sayan area, where the modern surface elevation reaches 700–800 m. Three blocks can be identified from maps of local gravitational field anomalies (*Figure 5.7*). In the central block, with gravitational fields varying from 0 to –20 milligals, rocks of granitoid composition, gneissic granite, and crystalline schists predominate. Flanking the central block are northeastern and southwestern blocks composed of more dense Archean–Proterozoic gneisses and schists, characterized by gravitation fields from 0 up to +15 milligals.

The location and morphology of interblock faults have been investigated in detail by Lukina (1994, 1996) as well as by Kupalov-Yaropolk *et al*. (1997). The following description is based on the work of these researchers. There are several faults in the region of the disposal area, as shown in *Figure 5.8*. Fault zones can be divided into two groups, ancient and modern, and are the most characteristic structural elements of the interfluvial geology (Lukina, 1994, 1996). Ancient faults are typically surface dislocations of Archean–Proterozoic intrusive-metamorphic sediments. Some ancient faults may have been rejuvenated in the Cenozoic era, possibly as late as the Quaternary period. Modern ruptures were created in the Quaternary period and displace late Pliocene surfaces. These faults divide the Yenisei–Kan interfluvial area into a series of relatively narrow tectonic blocks of submeridional (north–northwestern) strike. A stepwise increase from east (the Yeniseisk ridge of the Siberian platform) to west (the Siberian plate) of the Archean–Proterozoic metamorphic basement amounts to 1,600 m, and the Paleozoic basement depth increases in a similar fashion by a total of 1,300 m (Lukina, 1996). The primary faults near the disposal area are the Pravoberezhny (or “Right Bank”) fault to the west and the Telskii Byk fault to the north (see *Figure 5.8*).

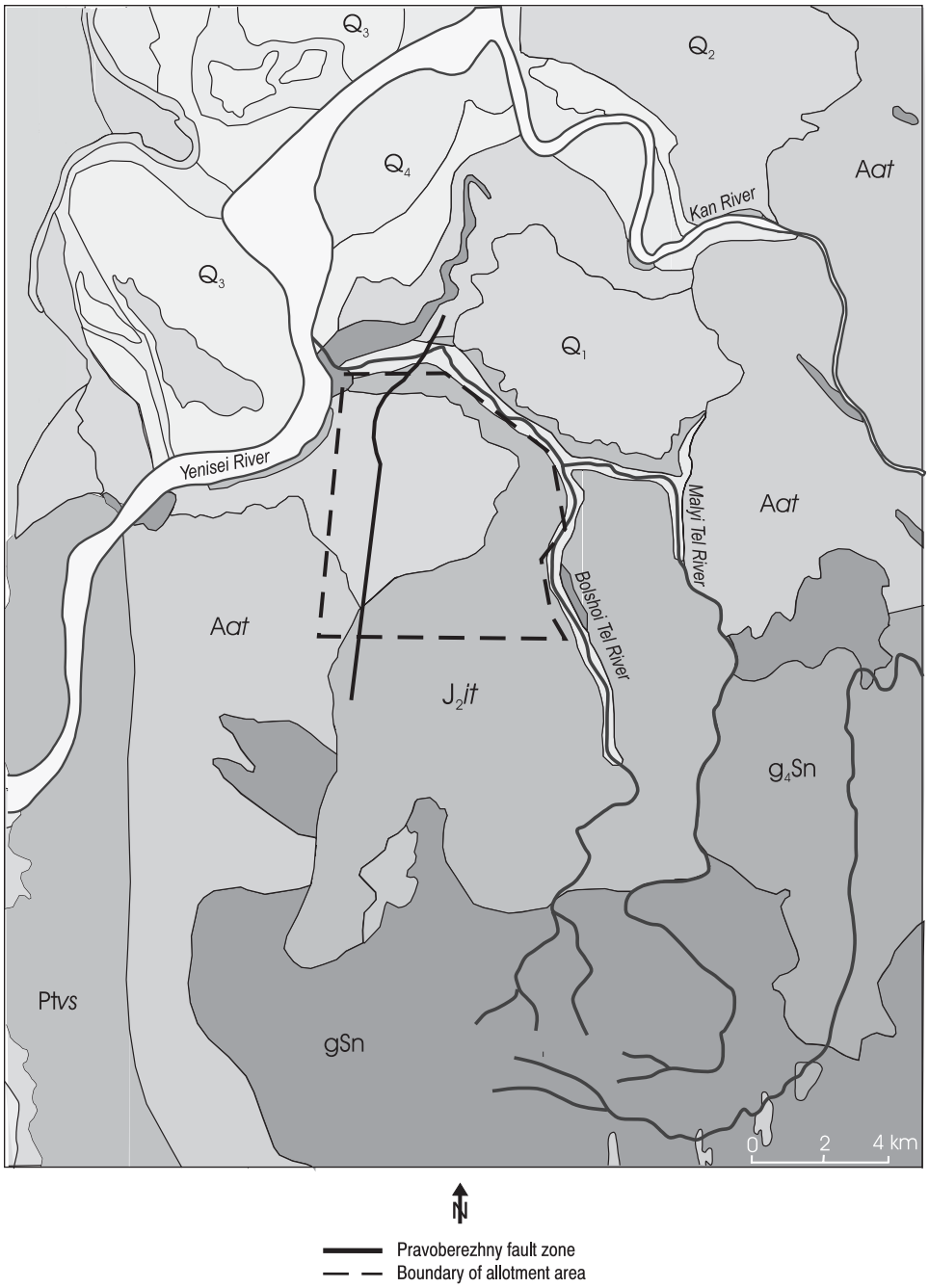

Figure 5.6. Geologic scheme of the Yenisei–Kan interfluvial area (redrawn from the 1963 Geologic map of the USSR) and position of the Pravoberezhny fault.

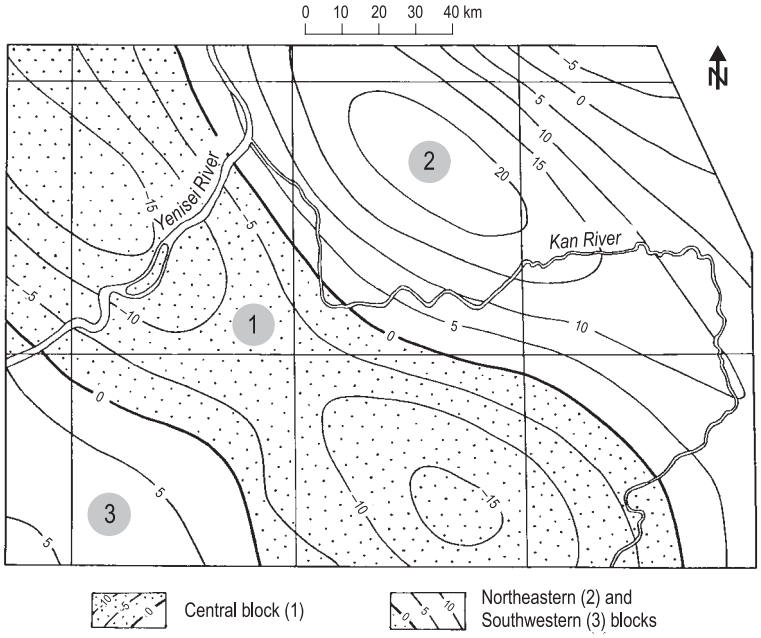

Figure 5.7. Map of the Yenisei–Kan interfluvial gravitational field anomalies for depth interval 12–25 km, in milligals.

The eastern boundary of the Yenisei–Kan interfluvial area is the north–northwest-striking Kan–Yenisei fault. This fault is reflected in the valleys of the Kan and Yenisei Rivers (*Figure 5.8*). A vertical Quaternary displacement of the late Pliocene surface can be distinctly traced along the fault, resulting in the uplift of the eastern block of the fault over the western block by approximately 250–290 m. Where the valley of the Kan River coincides with this fault, it has a canyon-like form and is characterized by steep slopes and a lack of terraces, thereby providing evidence of Quaternary tectonic movements. The Kan–Yenisei fault is distinctly marked by the zones of elevated horizontal gradients in gravitation fields (Vashchilov *et al.*, 1979). Gravimetric data indicate a fault depth of 25–34 km in the southern part of the interfluvial region, decreasing to 7.5–15 km in the northern part (*Figure 5.9*). The southern border of the Yenisei–Kan interfluvial area is the Iisk–Kan fault of west–northwest strike, separating the interfluvial region from the spurs of the Altai–Sayan region. The total vertical displacement of crystalline basement surfaces along this fault reaches 300–400 m. The fault can be seen in the modern relief as a sharply expressed scarp. The formation of this scarp occurred during the middle Pleistocene displacements of Yenisei River terraces, between

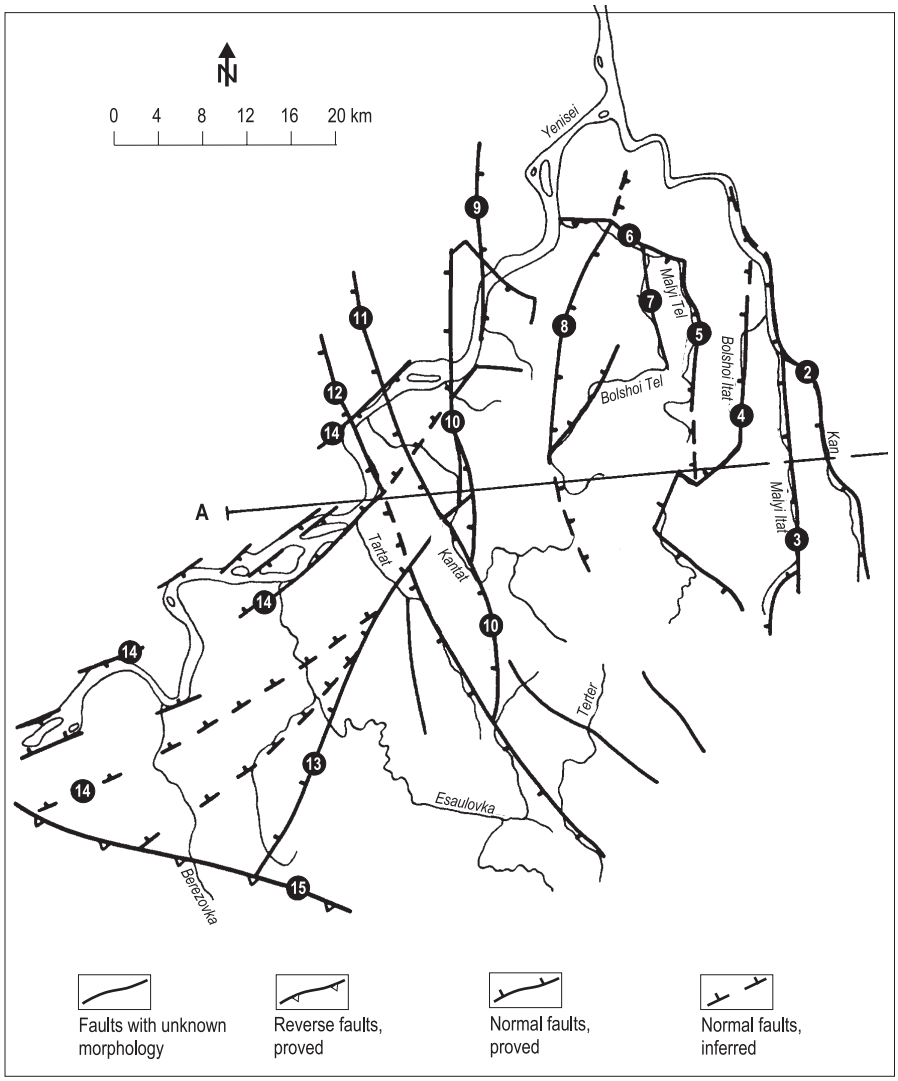

Figure 5.8. Fault lines in the vicinity of the Severny disposal site (after Kupalov-Yaropolk *et al*., 1997, and Lukina, 1994, 1996). Faults (figures in circles): (1) Iisk–Kan, (2) Kan–Yenisei, (3) Malyi Itat, (4) Bolshoi Itat, (5) Malyi Tel, (6) Telskii Byk, (7) Bolshoi Tel, (8) Pravoberezhny, (9) Atamanovsk, (10) Muratovsk, (11) Krasnoyarsk I, (12) Krasnoyarsk II, (13) Sosnovoborsk, (14) fragments of the Yenisei fault zone.

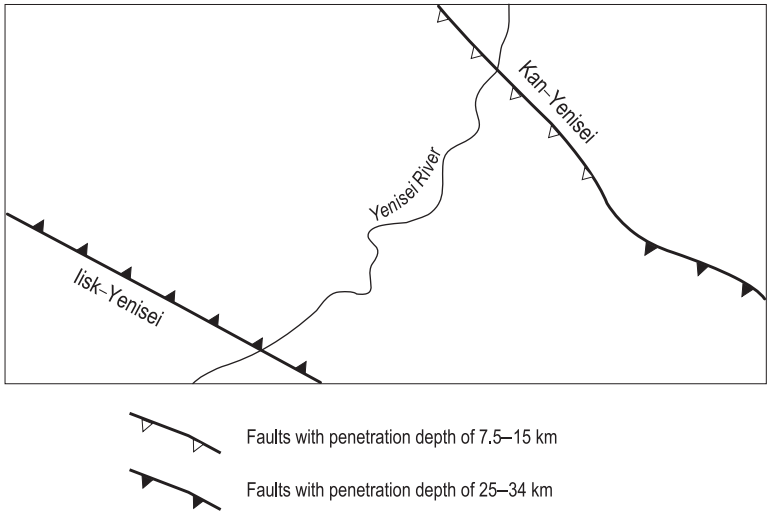

Figure 5.9. Location and depth of Kan–Yenisei and Iisk–Yenisei faults based on gravimetric data (Vashchilov *et al*., 1979).

130,000 and 200,000 years ago (Lukina, 1994). Neotectonic activity of the Iisk–Kan fault is also reflected in the morphology of the bed of the Yenisei River. In the southern fault wing the riverbed is narrow, with steep shores; in the northern wing the riverbed widens considerably, resulting in the presence of islands and river shallows. The Iisk–Kan fault is distinctly visible in gravitational field maps of the Yenisei–Kan interfluvial area as zones of elevated horizontal gravity gradients (see *Figure 5.7*). Gravimetric data indicate a fault depth of 25–34 km (Vashchilov *et al*., 1979). The northern boundary of the interfluvial region is the Yenisei fault, represented by a wide (4–5 km) band of echelon-like converged rupture disturbances striking northeast (*Figure 5.8*) along the valley of the Yenisei River. Vertical displacements are not marked along these ruptures, suggesting that the Yenisei fault originated under the influence of tectonic tension stresses (Lukina, 1996).

The Pravoberezhny fault, located in the western section of the interfluvial region has a submeridional strike. In the southern half of the Yenisei–Kan interfluvial area this fault forms the western boundary of a lower plate of granite–gneissic basement rocks. To the north, in the region of the injection site, the extent of Jurassic sediments increases sharply. These sedimentary deposits overlap not only the eastern crystalline basement rocks, but also the western blocks. However, based on drilling data (Rybalchenko *et al*., 1994), the thickness of Jurassic sediments in the western (upthrown) block is approximately 250 m, whereas in the eastern block the sediments are over 500 m deep. To the north of the disposal site allotment

boundary, the existence of a fault provisionally named the Telskii Byk fault has been proposed based on a number of geomorphological and geological signs. This fault strikes northwest along the valley of the Bolshoi Tel River. Interpretation of aerial photography of this valley indicates a vertical displacement of Quaternary deposits of approximately 50 m.

The Malyi Itat and Bolshoi Itat faults, also located in the western sections of the interfluvial region, are visible in the valleys of the Malyi Itat and Bolshoi Itat Rivers. Both faults are characterized by vertical displacements of late Pliocene formations of up to 60 m and 100 m, respectively. Activity of these faults during the Quaternary period has resulted in canyon-like valleys with steep slopes and a corresponding absence of terraces and floodplains. The depth of the Malyi Itat fault has been estimated by experts from Saint Petersburg University to be approximately 1.5 km.

The Malyi Tel fault occurs at the boundary between the two blocks and coincides with the valley of the Malyi Tel River. Granites and gneisses are exposed at the surface of the eastern block. In the western block, these rocks occur 350–380 m below the surface and are overlain by Jurassic sediments. In the modern relief, the fault is expressed by a distinct ledge that originated as a result of shifts during the late Pleistocene and Holocene epochs.

A group of converged conjugated fault zones of submeridional north–northwest strike (including the Atamanovsk, Muratovsk, Krasnoyarsk I, and Krasnoyarsk II faults) is located to the east of the Pravoberezhny fault (see *Figure 5.8*). All of these faults are sufficiently expressed in the geomorphology of the modern relief to be visible in satellite photographs. These faults separate structural blocks with various elevations of the crystalline basement (Lukina, 1994, 1996). The most considerable among them is Muratovsk fault, with a total vertical displacement reaching 500 m.

In summary, a series of submeridional faults, and a lesser number of northwest-striking faults, can be detected in the Yenisei–Kan interfluvial area on the basis of geomorphological, geological, and geophysical data. Displacements of ancient surfaces, layered Jurassic sedimentary rocks, and Quaternary sediments are observed along these faults, with the exception of the Yenisei fault. It is significant that these shifts at all of the faults investigated above are caused by vertical tectonic movements. The Pravoberezhny fault, investigated in particular in this report, is among these rupture structures. It is a linear mobile zone that has developed over a long period of time and has periodically been rejuvenated by tectonic movements in various periods of regional tectonic deformations, including the Quaternary. Therefore, the supposition of an adverse impact on the confining capacity of the Pravoberezhny fault as a result of longitudinal tectonic shifts that create “filtration windows” seems to be sufficiently substantiated.

5.1.3 Potential failure modes of the Pravoberezhny fault

The role that the Pravoberezhny fault zone plays in preventing flow toward the Yenisei River is discussed in Section 5.1.1. An evaluation of the mechanism, likelihood, and consequences of a disturbance of the isolating properties of the Pravoberezhny fault zone as a result of tectonic activity is important in evaluating the overall safety of the repository. Based on evaluation of available data, the IGEM report (IGEM, 1999b) concluded that the Pravoberezhny fault is most likely to suffer a loss of its confining properties as a result of either of two types of geological events:

- rejuvenation of the fault zone by longitudinal tectonic movements, with a consequent opening of filtration windows in the fault zone
- disruption of the continuity of the Pravoberezhny fault as a result of its being crossed by new or reactivated transverse faults.

These are discussed in more detail below.

Loss of the Confining Properties as a Result of Longitudinal Tectonic Movements

The research summarized here indicates that post-Jurassic vertical displacements in the disposal site region along the Pravoberezhny fault have amounted to more than 250–270 m. These displacements are substantiated by the sharp increase in the dip angle of the beds of Jurassic sediments in the immediate vicinity of the fault plane in both the eastern and western blocks (see *Figure 5.5*). The sedimentary layers indicate that post-Jurassic upthrusting tectonic shifts occurred in the plane of the Pravoberezhny fault. It is rather difficult to date these displacements more accurately. However, there are indications of neotectonic mobility of the Pravoberezhny fault. A 4–10 m scarp coinciding with the fault plane can be seen in modern relief (Lukina, 1994, 1996). Vertical shifting of early and later Holocene surfaces is visible along this scarp. The total amplitude of vertical displacements along the Pravoberezhny fault decreases to the north of the injection site, reaching only 75 m in the region of the Bolshoi Tel River. As noted above, based on the results of analyses of the Yenisei–Kan interfluvial area fault tectonics, vertical movements are the most probable rejuvenation mechanisms of the faults discussed here, including the Pravoberezhny fault. In the event the Pravoberezhny fault is activated, displacements would most likely occur along the most heterogeneous interior linear fault zones or along the plane of contact of the fault zone with the host rocks. In this case, significant degradation of the thin clay horizon that represents the ancient tectonic Pravoberezhny fault seam is not likely. Disturbances of this seam continuity may occur at places of fault flattening, where the clay horizon may be crushed and ruptured. This may result in the creation of filtration windows. Unfortunately, a

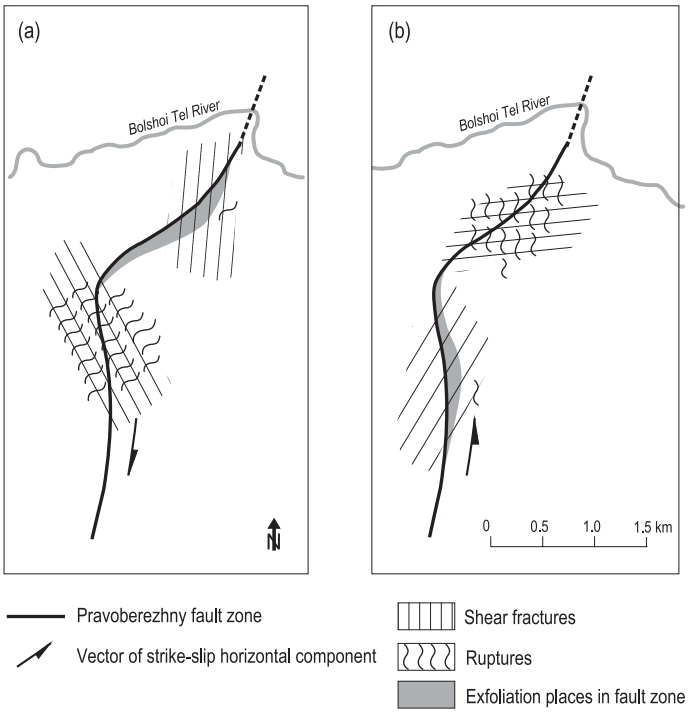

Figure 5.10. Fault zone failure during horizontal displacements: (a) southerly and (b) northerly displacement of downthrown block.

quantitative estimation for this scenario is not possible because of the lack of data on the deep morphology of the Pravoberezhny fault.

A more serious failure would occur if fault movements included a horizontal component in addition to the vertical displacement discussed previously. Such strike-slip fault movements could disturb seam integrity north of the injection zone, in the region where the Pravoberezhny fault displaces an arched bend (*Figure 5.10*). A horizontal strike-slip vector such as that noted in *Figure 5.10* could result in crushing, ruptures, and disintegration on one side of the bend, while the other side could experience exfoliation and formation of open cavities. A reversal of the strike-slip orientation would simply interchange the location of these types of failures. Depending on the magnitude of the horizontal strike-slip movement, the resulting disruption could extend several hundred meters along the fault zone. We caution that these evaluations are only rough approximations. Special investigations are necessary for more accurate determination of the degree of disturbance of the screen horizon.

Rupture of the Pravoberezhny Fault as a Result of its Displacement by a Transverse Rupture Disturbance

In addition to rejuvenation and vertical movements within the Pravoberezhny fault, failure of the confining ability of the fault zone could also occur as a result of its intersection by a transverse rupture disturbance caused by activation of the Telskii Byk fault. According to Lukina (1996), this fault crosses the Pravoberezhny fault zone near the northern boundary of the allotment area (*Figure 5.8*). Analysis of geologic and topographic maps of the region to the west of the Yenisei River shows that there are a number of linear elements of northwestern orientation in the current surface relief, in the separate river valley orientations, and in the geologic structures of this region. Thus it is possible that the Telskii Byk fault is continued to the west of the Pravoberezhny fault. Taking these data into account, it is not improbable that activation of the Telskii Byk fault may cause a continuity rupture of the Pravoberezhny fault at the point where these two faults intersect. Taking into account that the Pravoberezhny fault zone dips to the east, fault shifts along the Telskii Byk fault would lead to displacement of the section of the Pravoberezhny fault located to the south of the Telskii Byk fault. In this case, the displacement value would depend on the fault amplitude. The strike-slip displacement would depend on the orientation of the horizontal component. A rejuvenation could either increase or decrease the displacement. However, in either case, a continuity rupture of the Pravoberezhny fault could disturb the integrity of the clay seam that acts as a confining barrier.

5.2 Consequence Analysis

5.2.1 Input data and assumptions

The basic assumptions regarding the geology and hydrology of the site, waste data, and migration parameters used for this scenario are identical to those discussed in Chapter 4 for the inadvertent intrusion scenario. The only alteration made in conducting the fault zone failure analysis was a change in the transmissivity properties of the fault zone; all other assumptions, input data, and modeling are identical. However, there are few or no data on Horizon II in the region between the fault zone and the Yenisei River. The lack of adequate data in this region precluded modeling of consequences in Horizon II. However, it is important to note that the results of the inadvertent intrusion base case analysis indicate that the LLW in Horizon II is strongly sorbed and does not migrate far before it decays. It is expected that this conclusion would also have been reached for the scenario of a fault zone failure had sufficient data been available for modeling. However, in the absence of

data, we cannot make any conclusions regarding the impact of a fault zone failure on injected wastes in Horizon II.

The modeled conductivity of the fault zone was determined using a simple procedure. Based on the discussion above, it was assumed that the leakage through the fault zone that is hypothesized to be occurring at present is a function of the difference in the elevation of the upthrown and downthrown blocks. It was assumed that the head anomaly in the region of wells C-4 and C-36 represents a region of flow through the fault zone and that this flow window coincides with the minimum of the difference in elevations. A value of 10^{-4} m/d was given by VNIPIPT (1998) as the normal hydraulic conductivity of the fault zone. This value is over two orders of magnitude lower than the normal conductivity in the aquifer, which ranges between 0.3 and 1.6 m/d according to Rybalchenko *et al*. (1994). This results in a fault zone that is effectively a barrier to flow. Calibration of the conductivity of the fault zone was conducted on a trial-and-error basis. It was found that a maximum fault zone conductivity set at 3×10^{-3} m/d was adequate to reproduce the head anomaly observed in the region of wells C-4 and C-36, where the difference between the elevation of the upthrown and downthrown blocks is at a minimum. In order to develop a systematic approach that preserves the high resistance to flow in the disposal region while allowing heads to be reproduced more accurately in the northern section of the site, a simple log-linear relationship was then used to derive an expression for the relationship between the fault displacement and the hydraulic conductivity of the fault zone:

$$K = 0.003 \times 10^{-0.02 \times Z} \,, \tag{5.5}$$

where K is the hydraulic conductivity (in m/d) and Z is the difference in elevation between the roof of the downthrown block and the floor of the upthrown block (in m). It is important to note that this relationship is based on mathematical convenience rather than physical principles of fault zone morphology. It is simply a way to systematically preserve the integrity of the fault zone in areas where there is a large difference in the elevations of the upthrown and downthrown blocks while determining the likely areas of failure of the fault zone due to vertical displacement. A vertical displacement of the fault zone is assumed to bring the upthrown and downthrown blocks into hydraulic contact. There are other, and possibly more likely, failure modes of the fault zone, as discussed previously. However, the most likely areas of disruption for all potential failure mechanisms are in the northern and southern sections of the fault zone arch. These roughly coincide with the areas that would be affected by a vertical displacement, and therefore the model, which is simply based on altering the conductivity of the fault zone without reference to the mechanism by which the conductivity is altered, is still adequate for modeling purposes.

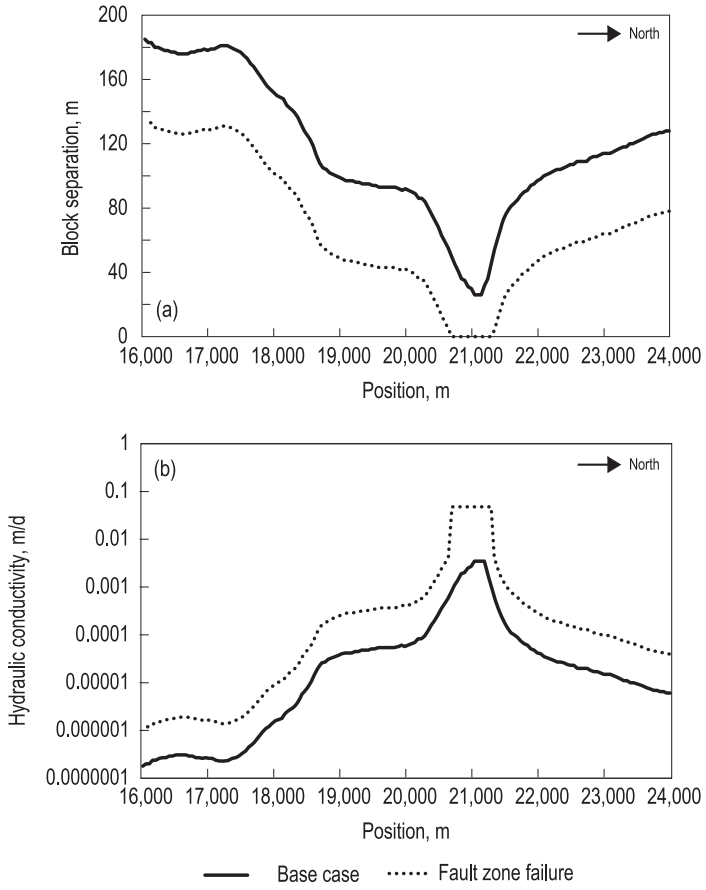

Figure 5.11. (a) Block separation and (b) modeled hydraulic conductivity along the fault zone.

The conductivities thus generated were used in the model for the base case to model the fault zone. It was assumed that the fault zone fails as a result of a vertical shift of 50 m, thus bringing the upthrown and downthrown blocks into direct contact. The area over which the contact is developed is thus a function of the relative difference in elevations. This can be seen in *Figure 5.11a*, showing the relative elevations before and after a shift of the fault zone. *Figure 5.11b* shows the hydraulic conductivity along the fault zone in both the base case and the fault zone failure scenarios. The conductivity of the fault zone was capped to be consistent with the hydraulic conductivity of the areas on either side of the fault zone. This results in the truncation of the hydraulic conductivity plot shown in *Figure 5.11b* to a maximum of 5×10^{-2} m/d. The number of cells in the fault zone affected by the shift is given in *Table 5.2*.

Table 5.2. Number of model cells affected by fault zone (assumptions).

Hydraulic conductivity, m/d	Maximum	$>10^{-2}$	$>10^{-3}$	$>10^{-4}$
Base case scenario	3×10^{-3}	0 (0%)	15 (9%)	34 (20%)
Fault zone failure scenario	3×10^{-2}	16 (9%)	29 (17%)	93 (55%)

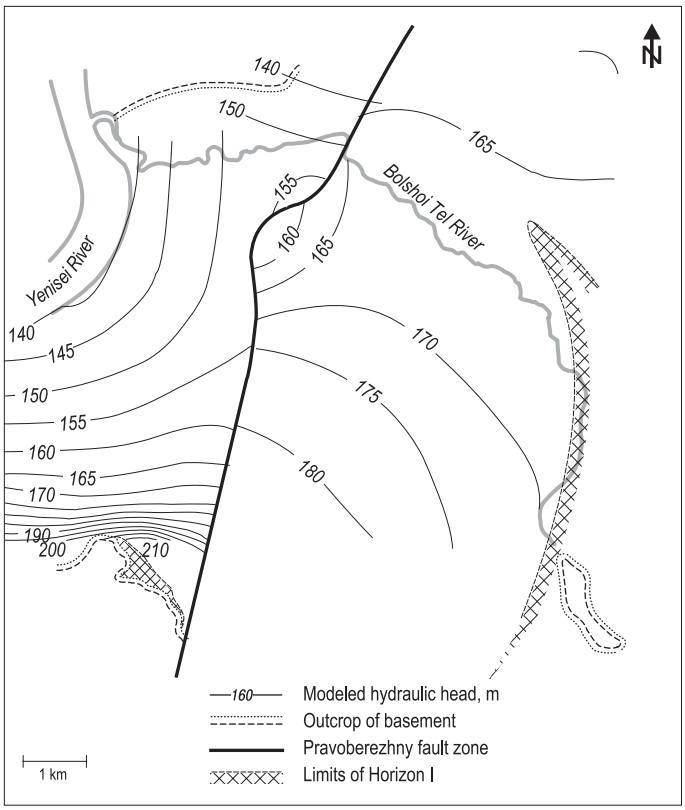

Figure 5.12. Modeled heads in Horizon I after failure of the fault zone.

Apart from the altered hydraulic conductivity of the fault zone, the input files for modeling were identical for both the base case and the fault zone failure scenarios.

5.2.2 Results

The results of hydraulic modeling of Horizon I are shown in *Figure 5.12*. One of the most important results is that, even though there is an order of magnitude shift and a large breach in the fault zone, the head patterns do not change dramatically

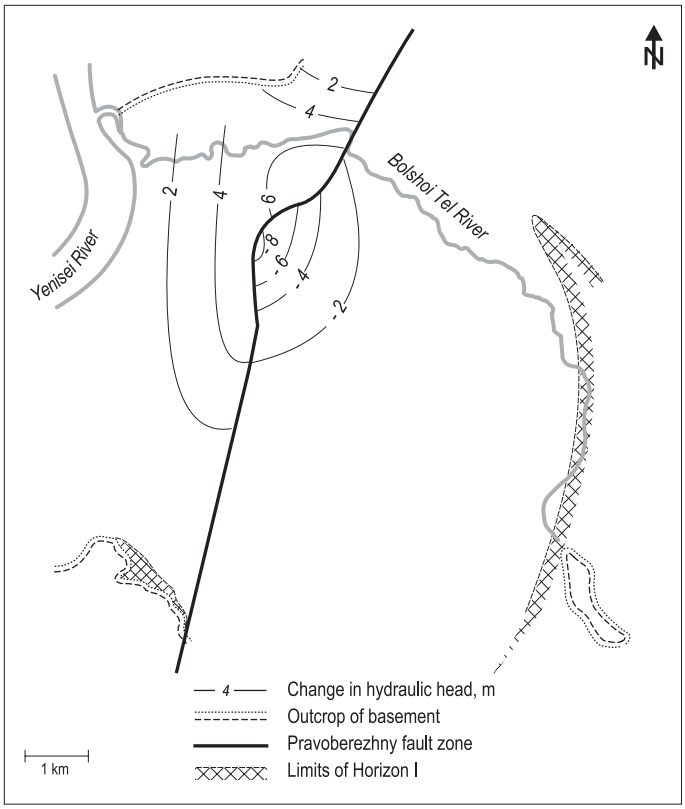

Figure 5.13. Change in modeled heads as a result of fault zone failure.

compared with the results from the base case modeling. This can be seen in *Figure 5.13*, showing the difference in the heads between the base case and the fault zone failure scenarios. The heads of the downthrown block in the immediate vicinity of the breach drop by as much as 10 m as a result of the increased discharge through the fault zone. However, away from the rupture, the head difference drops off, and there is very little change in modeled heads in the eastern section of the site, as seen in *Figures 5.12* and *5.13*. This is thought to be due to the very low transmissivity in the downthrown block north of the injection area between the disposal area and the area of postulated fault zone failure. The low transmissivities in this region may thus act as a "shield" that mitigates the effect of a breach in the fault zone, preventing it from having a widespread impact on the aquifer. This can also be seen in a velocity plot of the groundwater in Horizon I, shown in *Figure 5.14*.

The results of transport modeling are shown in *Figure 5.15*. The same methodology applied in the inadvertent intrusion scenario (see Chapter 4) is applied here. The doses from the individual radionuclides in both the HLW and the ILW are

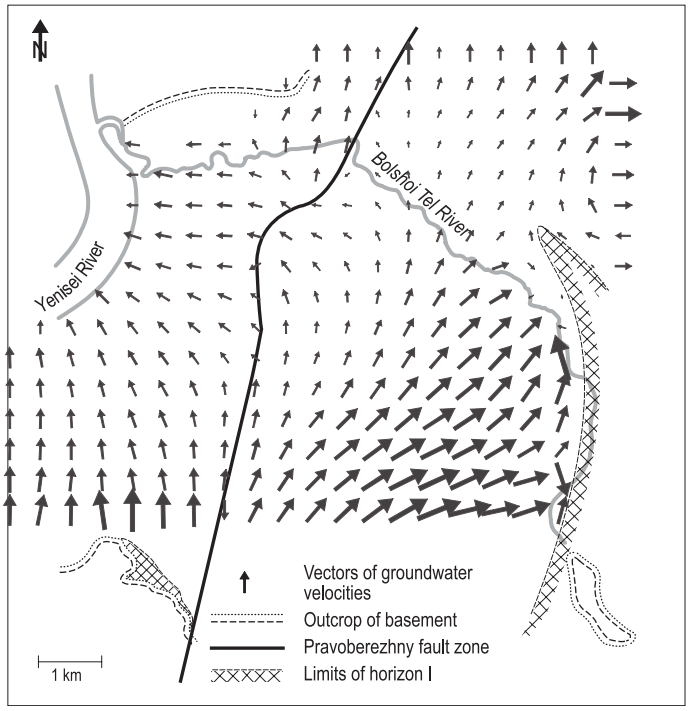

Figure 5.14. Magnitude and direction of groundwater velocity in Horizon I as a result of a fault zone failure.

summed at each point in the aquifer to give the total dose resulting from all radionuclides at each point in the aquifer. Dose contours are given for 1 mSv in *Figure 5.15a* and for 1 mSv, 10 mSv, 100 mSv, and 1 Sv in *Figures 5.15b* and *5.15c*.

The primary effect of a failure of the fault zone is the earlier arrival of the ^{99}Tc plume at the Yenisei River. It arrives at the Yenisei River at around 3,000 years and peaks between 3,000 and 10,000 years. In addition, a slight amount of ILW, injected into the eastern wells, is captured by the increased area of influence of the fault zone rupture. This results in a longer period of discharge into the Yenisei River. However, the sorbed contaminants do not reach the area of the fault zone rupture. Sorption will keep the plumes within the downthrown block for the next 10,000 years, although they will move slightly faster than in the intact fault zone scenario. The maximum intrusion doses (*Table 5.3*) are identical to those obtained in the base case intrusion report (cf. *Table 4.6*). For sorbed contaminants, there is no significant change in either the maximum concentration or the plume location. For nonsorbed (or weakly sorbed) contaminants, such as ^{99}Tc, the maximum concentrations are similar in both cases; only the location of the plume changes significantly.

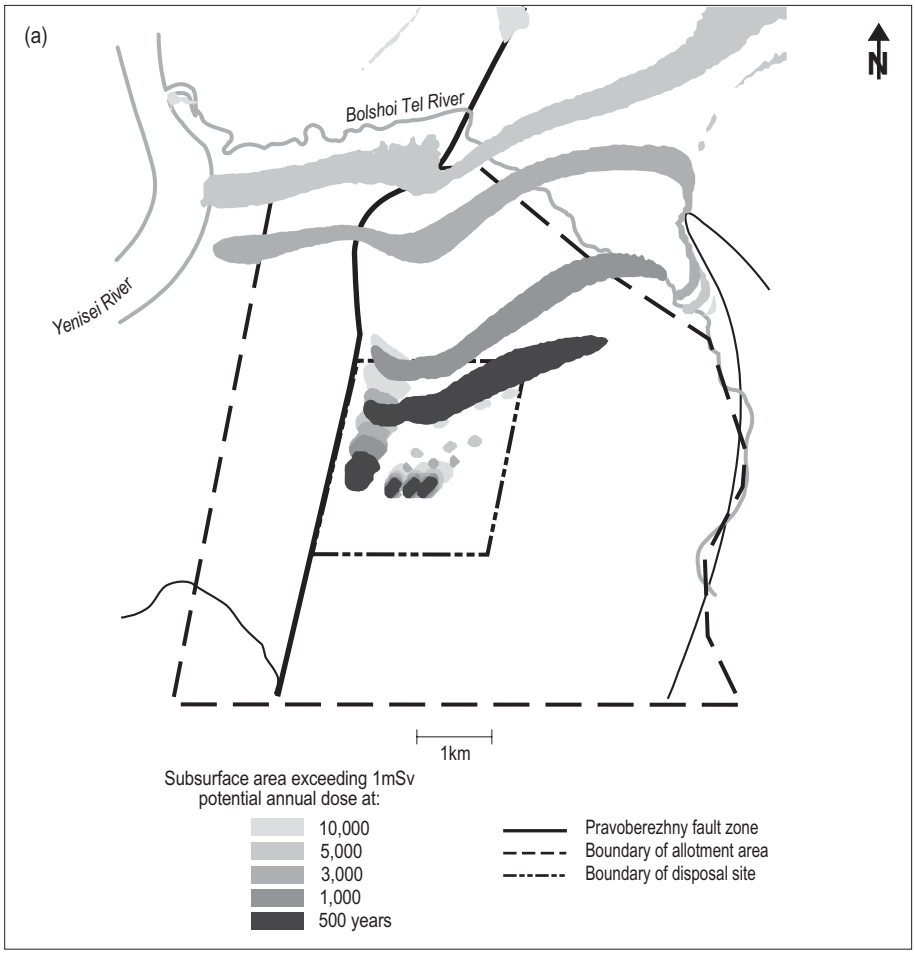

Figure 5.15. Horizon I intrusion doses after failure of fault zone: (a) from 500 to 10,000 years.

Doses were also calculated for the case of discharge to the Yenisei River. Only nonsorbed contaminants reach the Yenisei River boundary during the time frame of this analysis (10,000 years). A conservative approach similar to that taken in the Phase I report was used to estimate discharge into the river. Contaminants reaching the Yenisei River boundary and discharged in the constant head cells are assumed to be instantaneously advected into the river and mixed with the river flow. According to historical discharge data before the construction of the Krasnoyarsk dam (Kosmakov, 1996), the Yenisei River has an average annual flow of 2,920 m^3/sec, and an average minimum flow of 1,980 m^3/sec. In keeping with the conservative approach the average minimum annual flow was used as the river discharge. The

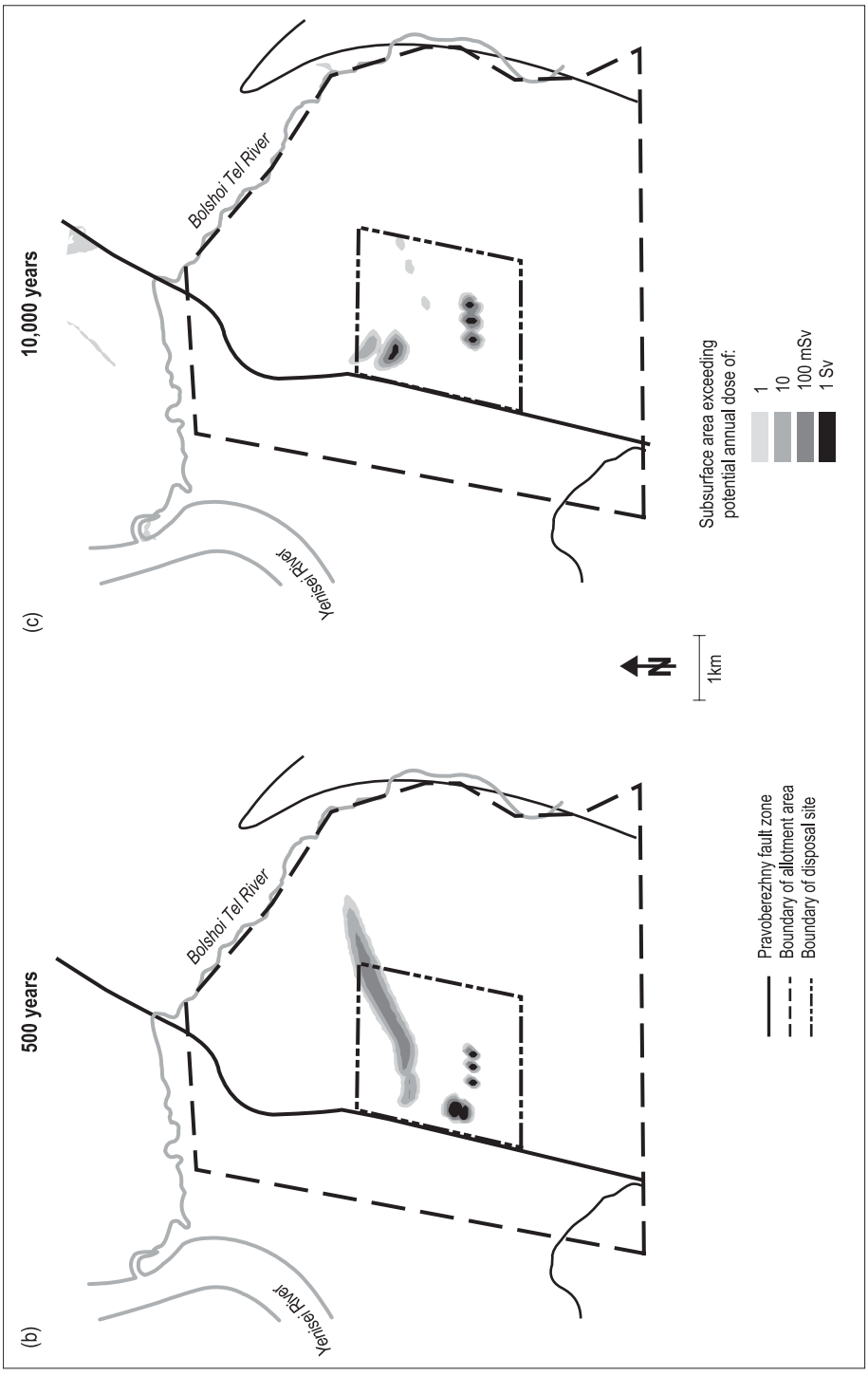

Figure 5.15 (continued). Horizon I intrusion doses after failure of fault zone: (b) 500 years; (c) 10,000 years.

Table 5.3. Maximum doses from ingestion of water from Horizon I after failure of fault zone, Sv/yr.

Radio-nuclide	500 years	1,000 years	3,000 years	5,000 years	10,000 years
^{241}Am	5.0E+01	2.2E+01	9.1E-01	3.7E-02	1.2E-05
^{135}Cs	1.8E-02	1.8E-02	1.8E-02	1.8E-02	1.8E-02
^{137}Cs	3.0E-01	2.8E-06	2.4E-26	2.1E-46	1.4E-96
^{237}Np	5.0E-01	5.0E-01	5.0E-01	5.0E-01	5.0E-01
^{239}Pu	2.7E+01	2.6E+01	2.5E+01	2.3E+01	2.0E+01
^{90}Sr	6.7E+00	4.5E-05	9.6E-26	2.0E-46	4.2E-98
^{99}Tc	1.5E-01	1.5E-01	1.5E-01	1.5E-01	1.4E-01

annual flow, rather than the monthly flow, is used, as the dose limit is calculated on an annual basis. The same caveats apply to this analysis as applied to the Phase I study. This analysis yields a maximum upper bound on the concentration in the river water, not a best estimate of the concentration. Because of the much greater discharge in the Yenisei River, the maximum annual doses will be much lower than the values calculated for the Bolshoi Tel in Phase I, reaching a maximum of only 7.2×10^{-10} Sv, far below the 1 mSv annual dose limit specified in NRB-96 (1996).

5.3 Conclusions

Based on the preceding analysis, the primary effect of a failure of the fault zone would be the earlier arrival of the ^{99}Tc plume in the upthrown block and at the Yenisei River, and a longer period of discharge into the Yenisei, as the breach in the fault zone captures a portion of the ILW plume. The most likely area for a failure of the fault zone is the section approximately 3–4 km north of the injection site, in the area of the arched bend of the existing fault zone. The maximum doses would not be significantly changed, although changes in the location and arrival time of peak doses would occur.

6
Conclusions and Recommendations

6.1 Inadvertent Intrusion Scenario

1. *The consequences of an inadvertent intrusion into Horizon I will lead to doses several orders of magnitude above the current 1 mSv dose limit (specified in NRB-96, 1996) for at least the next 10,000 years, and for potentially much longer. Institutional controls, by themselves, are insufficient to prevent unacceptable exposures. However, the likelihood of such an intrusion is low owing to the effort required to reach the areas of contamination and the availability of more attractive groundwater resources at much shallower depths.*

The consequences of an intrusion into Horizon I, considered under the worst possible case (location of a drinking-water well directly in the region of the injection site), would lead to unacceptable doses for over 10,000 years. This dose would be due to the long-lived transuranic radionuclides – primarily ^{239}Pu and ^{241}Am for the next several thousand years, and ^{239}Pu and ^{237}Np after 10,000 years. A highly conservative estimate results in a maximum annual dose of over 10 Sv per year, as seen in *Figure 4.3* and in *Table 4.6*.

However, the likelihood of this event is low. Although the groundwater in Horizon I is fresh, and thus suitable for drinking water, the transmissivity of the aquifer is too low to sustain a large drinking-water system, for which transmissivities exceeding 100 m^2/d are generally required. Therefore, the only feasible sustainable well in Horizon I would likely be a small community well. In addition, in drilling a well in the area of maximum risk, one would encounter potable groundwater in Horizon III at far shallower depths. There is no reason to assume that a potable water well would bypass the usable water in Horizon III and, after several hundred years, the usable groundwater in Horizon II, and attempt to exploit the far deeper Horizon I. Finally, the areas resulting in high doses are small, and the likelihood that a well would be so precisely placed as to hit the peak of a contaminated plume is therefore small, even if such a well were attempted (areas of potential hazard are

shown in *Figure 4.6*). Therefore, the likelihood of exposure to the high groundwater concentrations in Horizon I is very low, and the risk posed by the contaminated groundwater in Horizon I, being a function of both consequence and probability, is thus low.

2. *The consequences of an inadvertent intrusion into Horizon II could result in doses above the current 1 mSv annual limit (specified in NRB-96, 1996) for a period of a few hundred years. Institutional controls would need to remain effective for approximately 300 years. However, although the likelihood of an intrusion into Horizon II is higher than that of an intrusion into Horizon I, it is still low.*

The values of maximum doses resulting from intrusion into Horizon II are presented in *Table 4.7* and in *Figure 4.5*. After 300 years, only ^{239}Pu is capable of resulting in annual doses above 1 mSv, and even that is conservatively estimated to be only 7.3 mSv.

As Horizon II is shallower than Horizon I, there is a somewhat higher risk of intrusion. However, this risk is still low, as discussed in Section 4.2. Horizon III appears to overlie Horizon II in the area where the ^{239}Pu is expected to remain; if that aquifer is a usable source of drinking water, there is no reason to believe that water well exploration would continue below it. The long-term risk due to the LLW in Horizon II therefore appears to be slight, as only ^{239}Pu will remain in levels above drinking-water standards after 300 years and the likelihood of intrusion is low.

3. *The presence of Horizon III, which acts as a buffer, is an important factor in limiting the likelihood of an inadvertent intrusion into the contaminated deeper horizons. Care should be exercised in decommissioning the site to prevent contamination of this groundwater resource. In addition, monitoring of the waters of Horizon III would provide an early indication of the potential for unacceptable doses due to an inadvertent intrusion. A more rigorous evaluation of the potential for contamination of Horizon III would allow adequate plans to be put in place to prevent contamination.*

The analysis of the likelihood of exposure indicates that the presence of Horizon III could be important in reducing the probability of intrusion of deeper aquifers for groundwater use. This aquifer overlies the regions where the majority of the long-lived radionuclides will be retained and therefore would be encountered by an exploratory water well before the wastes were contacted. If this aquifer is a usable source of drinking water, there is little reason to expect continued exploration below

it. The aquifer lies at much shallower depths and is thus within the reach of conventional water-well technology for a domestic well. Horizon III is thus a highly valuable buffer against inadvertent intrusion into the deeper disposal horizons. If it can be shown that this is a usable water supply, then the chances of intrusion into the deep aquifers are greatly reduced.

However, the attractiveness of Horizon III as an underground source of drinking water also implies that it is important to protect it from contamination. It is difficult to assess the potential for pollution of Horizon III. However, in the worst case, a failure in the sealing or casing of a well penetrating Horizon III and in communication with the deeper horizons could represent a viable pathway for contaminant migration. If the head gradient and degree of failure of the casing are such that contaminated groundwater flows up into Horizon III, a significant possibility of exposure may result.

4. *The plume of long-lived transuranic radionuclides formed by HLW and ILW injection is likely to persist for thousands of years, retaining roughly the same geometry and migrating very slowly. Therefore, the maximum dose in the future is proportional to the maximum concentration formed in the present. Detailed modeling of the formation of the transuranic plume and subsurface monitoring for long-lived constituents will therefore allow a much improved assessment of the consequences of intrusion in the future.*

In these analyses, the exposure path selected for analysis is the placement of a drinking-water well in the contaminated plume and the subsequent use of the contaminated groundwater as the sole source of drinking water. Agricultural pathways (irrigation and livestock watering) were not taken into account in estimating doses.

The analysis conducted here used the conservative estimate that the subsurface concentration of long-lived radionuclides was equal to the concentration of these radionuclides in the injected waste. However, the wastes may be dispersed as they are injected, and waste interaction with the repository rock will alter the aqueous phase concentrations. Over the long term, changes in the geochemical conditions in the subsurface as the chemical conditions reach long-term equilibrium have the potential to reduce maximum aqueous phase concentrations in the aquifer to below those in the injected wastes. An analysis of the formation of the plume focused on the hydrology and geochemistry of the disposal area itself will provide a much more accurate estimate. Such an effort could be validated with field measurements from wells in or near the disposal site, yielding a high degree of confidence in the results. In addition, investigation of potential long-term changes in the subsurface chemistry may provide insight into the changes in doses to a hypothetical intruder after institutional controls fail.

6.2 Fault Zone Failure Scenario

1. *The barrier efficiency of the fault zone appears well substantiated in the area of injection operations. The evidence for the confining ability of the fault zone farther to the north is unclear. However, even if the barrier efficiency is impaired several kilometers to the north of the fault zone, the radiological consequences of discharge to the Yenisei River are minor. The maximum annual doses due to ingestion of drinking water contaminated by discharge of wastes to the Yenisei River are expected to be several orders of magnitude below the current 1 mSv dose limit (specified in NRB-96, 1996) for at least the next 10,000 years.*

There is substantial evidence for the confining ability of the fault zone in the area of the disposal site, as discussed above. This includes the difference in static water levels across the fault zone, the degree of vertical displacement, and the experience of injection operations in which changes in heads across the fault zone are not observed in the region of waste disposal. However, several pieces of evidence point to a gradual degradation in the confining ability of the fault zone farther to the north. These include the water heads in northern wells located near the fault zone, as well as geological maps showing a lower magnitude of vertical displacement. However, even a failure of the fault zone in this region would not result in doses above the 1 mSv annual dose limit. A large failure would cause contamination to arrive in the Yenisei several thousand years sooner than in the base case scenario, as seen by a comparison of *Figures 4.3* and *5.15*. The high discharge in the Yenisei River will result in doses far lower than the current 1 mSv annual dose limit. This dose is due only to the nonsorbed contaminant ^{99}Tc. Long-lived transuranic radionuclides will be retained in the downthrown block for over 10,000 years.

2. *Failure of the fault zone will not lead to a significant change in the potential maximum intrusion doses received in the future, although it will affect the location and time that such doses might be received.*

A comparison of the dose plots in *Figure 5.15* with those in *Figure 4.3* shows that the western wastes will migrate faster in the event of a failure of the fault zone and will reach the Yenisei River several thousand years sooner. However, the maximum intrusion doses are not affected. Furthermore, a failure of the fault zone as modeled does not significantly affect wastes discharged near the eastern boundary of the disposal area, as can be seen in the dose plots. Only a small portion of the wastes injected in the eastern wells will be drawn through the failed area of the fault zone.

6.3 Summary

Density-driven flow dominates regional groundwater flow patterns for dense waste as in Horizon I. Therefore, modeling of the migration of dense wastes is not highly sensitive to uncertainties in the porosity or the transmissivity of the aquifer. The dense saline wastes are expected to settle in the depression north of the disposal area. However, the time required for leakage through the confining layer between Horizon I and Horizon II is sensitive to changes in the measured values of transmissivity. Travel time may be as short as 1,000 years if the measured transmissivity values are lower than the actual values by a factor of two. This result underscores the need for a better understanding of the potential hydraulic interaction between the two aquifers in the northeastern section of the disposal area.

None of the hypothetical scenarios investigated poses a substantial risk to the public in the short term. The long-term situation is less clear. Use of Horizon I waters for drinking water could have severe consequences for the foreseeable future (over 10,000 years), with annual doses well over 1 Sv possible. More refined estimates of maximum potential drinking-water doses would require a better understanding of the dynamics of plume formation as a result of injection and the geochemical changes that will occur as the aquifers reach a new geochemical equilibrium. However, the likelihood is judged to be slight because of the depth to the groundwater and the presence of more attractive groundwater resources in the river valleys.

The mobility of ^{99}Tc may result in subsurface concentrations in Horizon I near potential discharge areas well above current regulatory limits. However, the ^{99}Tc would have to migrate vertically to reach areas where a well may be located. A better understanding of the dynamics of discharge from the horizons to overlying aquifers may clarify the significance of ^{99}Tc.

A fault zone failure would not increase the risks posed by the site. Although contamination of the Yenisei River could occur under this scenario, doses resulting from the use of contaminated water from the Yenisei River are more than six orders of magnitude below the currently acceptable 1 mSv annual dose limit specified in NRB-96 (1996). This is primarily due to the enormous dilution potential of the Yenisei River as compared with the Bolshoi Tel River.

Based on the analyses presented here, the deep well injection site at the MCC does not appear to present a major short-term risk of public exposure or of significant contamination of the surface waters given the current understanding of environmental conditions. This is due primarily to the low groundwater velocities, the degree of sorption that may reasonably be expected at the site, and the potential dilution of contaminated groundwater with surface water. The most significant long-term risk appears to be the potential for use of contaminated groundwater for drinking water after the loss of institutional control of the site.

Appendix I

Appendix I is not included in the printed version of this report because of space constraints. Interested readers may consult either Chapter 2 of Volume I of this report (Compton, K.L., Novikov, V., and Parker, F.L., 2000, *Deep Well Injection of Liquid Radioactive Waste at Krasnoyarsk-26: Volume I*, RR-00-01, International Institute for Applied Systems Analysis, Laxenburg, Austria), or the electronic version of this report, available online at the RAD Project home page: www.iiasa.ac.at/Research/RAD.

Copies are also available from IIASA's Publications Department.

References

Compton, K.L., Novikov, V., and Parker, F.L., 2000, *Deep Well Injection of Liquid Radioactive Waste at Krasnoyarsk-26*, Vol. I, RR-00-1, International Institute for Applied Systems Analysis, Laxenburg, Austria.

Driscoll, F., 1986, *Groundwater and Wells*, 2nd ed., Johnson Filtration Systems Inc., St. Paul, MN, USA.

Fetter, C.W., 1988, *Applied Hydrogeology*, 2nd ed., Macmillan Publishing Company, New York, NY, USA.

Freeze, R.A., and Cherry, J.A., 1979, *Groundwater*, Prentice Hall, Inc., Englewood Cliffs, NJ, USA.

Golden Software, Inc., 1996, Surfer (Win 32)®, Version 6.04, Golden, CO, USA.

Goncharov, A.V., and Krivocheev, V.P., 1966, Report on hydrological investigations, site "B," 1964–1966, GGP *Hydrospesgeologia*, Krasnoyarsk, Russia.

Goncharov, A.V., and Krivocheev, V.P., 1967, Report on detailed hydrological investigations of discharge area of Horizon I, GGP *Hydrospesgeologia*, Krasnoyarsk, Russia.

Goncharov A.V, and Nosukhin, A.V., 1963, Report on exploration work and hydrological investigations in site "Pravobereznii," GGP *Hydrospesgeologia*, Krasnoyarsk, Russia.

Goncharov, A.V., and Nosukhin, A.V., 1965, Report on hydrological mapping of site "B," scale 1:50000, GGP *Hydrospesgeologia*, Krasnoyarsk, Russia.

Harbaugh, A.W., and McDonald, M.G., 1996, User's Documentation for MODFLOW-96, An Update to the US Geological Survey Modular Finite-Difference Ground-water Flow Model, US Geological Survey Open-File Report 96-485, USGS, Reston, VA, USA.

ICRP (International Commission on Radiological Protection), 1996, Age-Dependent Doses to the Members of the Public from the Intake of Radionuclides, Part 5, Compilation of Ingestion and Inhalation Coefficients, ICRP Publication 72, *Annals of the ICRP*, **26**(1), Pergamon, Oxford, UK.

IGEM (Institute of Geology of Ore Deposits, Petrography, Mineralogy and Geochemistry), 1997, Conceptual Approach to Modeling of LRW Migration from the MCC Disposal Site: Comparison Studies of Contaminant Transport Driving Forces, Moscow, Russia.

IGEM (Institute of Geology of Ore Deposits, Petrography, Mineralogy and Geochemistry), 1998a, Preliminary Analysis of Groundwater Hydrology at the MCC Deep-Well Injection Site (Progress Report, February 1998), IGEM, Moscow, Russia.

IGEM (Institute of Geology of Ore Deposits, Petrography, Mineralogy and Geochemistry), 1998b, Preliminary Analysis of Groundwater Hydrology at the MCC Deep-Well Injection Site (Progress Report, May 1998), Moscow, Russia.

IGEM (Institute of Geology of Ore Deposits, Petrography, Mineralogy and Geochemistry), 1999a, Sensitivity Analysis of Transmissivity and Leakage Distribution in Horizon I (Progress Report, February 1999), IGEM, Moscow, Russia.

IGEM (Institute of Geology of Ore Deposits, Petrography, Mineralogy and Geochemistry), 1999b, Disjunctive Tectonics of Yenisei-Kan Interfluvial Region and Analysis of the Pravoberezhny Fault Zone Geology (Progress Report, March 1999), IGEM, Moscow, Russia.

Konikow, L.F., Goode, D.J., and Hornberger, G.Z., 1996, A Three-Dimensional Method-of-Characteristics Solute-Transport Model (MOC3D), US Geological Survey Water-Resources Investigations Report 96-4267, US Geological Survey, Reston, VA, USA.

Kosmakov, E.V., 1996, Determination of Possible Places of Radioactive Contamination of River Yenisei Valley between Villages of Atamanovo and Strelka (Based on Analysis of Hydrological Processes), Scientific and Research Enterprise on Natural Systems Ecology (EPRIS), Divnogorsk, Russia.

Kupalov-Yaropolk, O.I., *et al*., 1997, Prediction of environmental risks of disposal of liquid radioactive wastes in the junction zones between platforms and foldbelts, *Geoecology*, **5**:60–74.

Lukina, N.V., 1994, Quaternary Fault Tectonics of the Junction Zone between the Siberian Platform and West Siberian Plate in the Yenisei–Kan Interstream Area, abstract of presentation at the All-Russian Conference on the Study of Quaternary Period, Moscow, Russia, p. 147.

Lukina, N.V., 1996, Active faults in the junction zone between the Siberian platform and Altay–Sayan Orogenic belt, *Bulletin of the Moscow Society for Nature Testers, Section Geology*, **71**(5):25–32.

Matthess, G., 1982, *The Properties of Groundwater*, Wiley Interscience, New York, NY, USA.

McDonald, M.G., and Harbaugh, A.W., 1988, A Modular Three-Dimensional Finite-Difference Ground-Water Flow Model: US Geological Survey Techniques of Water-Resources Investigations, Book 6, Chap. A1, US Geological Survey, Reston, VA, USA.

NRB-96, 1996, Norms of Radiation Protection 96, Energoatomizdat, Moscow, Russia.

Parker, F.L., Rybalchenko, A.I., Velichkin, V.I., Compton, K.L., Novikov, V.M., Pek, A.A., Malkovsky, V.I., and Sigaev, B.P., 1999, Analysis of long-term consequences of deep well injection disposal of liquid radioactive waste at the Mining and Chemical Combine, Krasnoyarskii Krai: I. Normal evolution scenario, *Geology of Ore Deposits*, **41**(6):423–439.

Parker, F.L., Rybalchenko, A.I., Velichkin, V.I., Compton, K.L., Novikov, V.M., Pek, A.A., Malkovsky, V.I., Asadulin, E.E., and Sigaev, B.P., 2000, Analysis of long-term consequences of deep well injection of liquid radioactive waste at the Mining Chemical Combine, Krasnoyarsk Krai: II. Hypothetical scenarios, *Geology of Ore Deposits*, **42**(2):111–127.

Rybalchenko, A. I., Pimenov, M.K., Kostin, P.P., Balukova, V.D., Nosukhin, A.V., Mikerin, E.I., Egorov, N.N., Kaimin, E.P., Kosareva, I.M., and Kurochkin, V.M., 1994, *Underground Disposal of Liquid Radioactive Wastes*, IZDAT, Moscow, Russia (in Russian). English Translation by Ben Teague, Sandia National Laboratories, January 1996. Published in 1998 as Rybalchenko, A.I., ed., 1998, Deep Injection Disposal of Liquid Radioactive Waste in Russia, Battelle Memorial Institute, Richland, WA, USA.

Tsang, C.F., 1996, Some hydrological factors affecting the safety of deep injection disposal of liquid wastes, in J.A. Apps and C.F. Tsang, eds, *Deep Injection Disposal of Hazardous and Industrial Waste: Scientific and Engineering Aspects*, Academic Press, New York, NY, USA.

Vashchilov, Y.N., *et al*., 1979, Interpretation of gravity anomalies of the Yenisei Ridge and adjoining regions on the basis of the Lithosphere's Blocky-Bedding Model, *Geology and Geophysics*, Nauka, Novosibirsk, Russia (in Russian).

VNIPIPT (All-Russian Research and Design Institute of Production Engineering), 1998, Preparation of the Data for Evaluation and Modeling of Impact of Deep Well Injection of Liquid Radioactive Waste of Mining and Chemical Combine, VNIPIPT, Moscow, Russia.

VNIPIPT (All-Russian Research and Design Institute of Production Engineering), 1999, Report on Stage 3 of IIASA Project "Evaluation Study," (a)Analysis of Fault Zone Geology near Deep Storage for Liquid Radioactive Waste of Mining and Chemical Combine, (b) Feasibility of Groundwater Exploitation in Horizon I and Horizon II Groundwater Potability Characteristics, Technical Requirements for Well Emplacement in Horizon I and II, (c) Site Decommissioning Plan for Deep Storage for Liquid Radioactive Waste of Mining and Chemical Combine: Basis Conception, VNIPIPT, Moscow, Russia.

Further Reading

AEA Technology, 1997, Measurements, modelling of migration and possible radiological consequences at deep-well injection sites for liquid radioactive waste in Russia, European Commission EUR 17626 EN.

Apps, J.A., and Tsang, C.F., eds, 1996, *Deep Injection Disposal of Hazardous and Industrial Waste: Scientific and Engineering Aspects*, Academic Press, San Diego, CA, USA.

Bradley, D.J., 1997, *Behind the Nuclear Curtain: Radioactive Waste Management in the Former Soviet Union*, D.R. Payson, ed., Battelle Press, Columbus, OH, USA.

Cochran, T.B., Norris, R.S., and Bukharin, O.A., 1995, *Making the Russian Bomb – From Stalin to Yeltsin*, Westview Press, Boulder, CO, USA.

Egorov, N., ed., 1998, Nuclear Inheritance of the Former Soviet Union. Sector Overview, report of IIASA RAD Project and ISTC project #245, International Institute for Applied Systems Analysis, Laxenburg, Austria.

Kondratyev, A.N., Martynov, Y.P., and Strakov, M.V., 1976, Management of High-Level and Alpha-Emitting Waste in the USSR, International Atomic Energy Agency, Vienna, Austria.

Nikipelov, B.V., Suslov, A.P., and Tsarenko, A.F., 1990, Radioactive Waste Management in the USSR: Experience and Perspective, Waste Management 90 conference, Tucson, AZ, USA.

Robinson, S., and Volosov, A., eds, 1996, *Radioecology of the Southern Part of Krasnoyarsk Region in the Impact Zone of the Mining Chemical Combine (Zheleznogorsk)*, Green Cross Russia, Moscow, Russia.